SUPERCONDUCTING ORDER PARAMETER DOMAINS IN Sr_2RuO_4 PROBED BY JOSEPHSON INTERFEROMETRY

BY

FRANCOISE KIDWINGIRA

Licence, Université du Burundi, 1999
M.S., Clark Atlanta University, 2001

DISSERTATION

Submitted in partial fulfillment of the requirements
for the degree of Doctor of Philosophy in Physics
in the Graduate College of the
University of Illinois at Urbana-Champaign, 2007

Urbana, Illinois

Abstract

There is evidence for degenerate chiral order parameters of $p_x \pm ip_y$ symmetry in the superconducting ruthenate Sr_2RuO_4 which can lead to the presence of chiral order parameter domains in the material. We study bi-metallic Josephson junctions made of Sr_2RuO_4 and a conventional superconductor. Their critical current modulations in an applied magnetic field carry information about the phase of the order parameter of the ruthenate. In these junctions, we observe multiple phase interference in a single tunneling direction which indicates the presence of order parameter domains. The domain structure creates in some samples a striking qualitative difference between the magnetic field modulations of the critical current of junctions fabricated on orthogonal faces of a Sr_2RuO_4 single crystal. Transitions between the chiral states of a domain or motion of domain walls separating them generates telegraph noise in the critical current as a function of either magnetic field or time, and is responsible for hysteresis observed in field sweeps of the critical current. Cooling the junctions in a magnetic field lifts the degeneracy between the two types of domains. The increased probability of one chirality over the other translates into an enhanced critical current for the junctions. The presence of such domains confirms the suspected p-wave spin triplet and complex nature of the superconducting pairing state in Sr_2RuO_4, making it the superconducting analog of the A-phase of superfluid ^3He.

To Charles, for his love and support
and to Alec for bringing so much joy in my life

Acknowledgments

I would like to thank my advisor Professor Dale J. Van Harlingen, an outstanding researcher and excellent teacher. It has been a privilege to work in his group and I have learned so much from him. I would also like to thank the entire DVH group for creating a pleasant work environment. I thank William Neils and Tony Bonetti for training me when I started in the group, Trevis Crane and Sergey Frolov for answering so many of my questions, Madalina Colci O'Hara, Micah Stoutimore, David Caplan, Dan Bahr, Martin Stehno for their friendship, useful discussions, and availability when I needed help. Particular thanks to Joel Strand whom I've been working closely with and who came up with the polishing procedure we used in the present work. I am grateful to Professor Yoshiteru Maeno and his group at Kyoto university for sending us some of the best Sr_2RuO_4 crystals in the world. My thanks also to the MRL staff and its facilities, especially Tony Banks at microfab for providing the technical support I needed in my work.

Although I can't possibly thank all the people who have made it possible for me to be getting this degree, I would like to acknowledge my family for their unconditional support and two of my mentors: Professor Romain Murenzi whose invaluable help and advice was essential to my coming to the United States for graduate school and Professor Alfred Msezane, my master's thesis advisor.

Finally, I would like to acknowledge the funding agencies for financial support: the NSF grant DMR-01-07253 and the Department of Energy, Office

of Basic Energy Sciences, grant DEFG02-91- ER45439 through the Frederick Seitz Materials Research Laboratory at the University of Illinois at Urbana-Champaign.

Table of Contents

List of Figures

1 Introduction

Superconductivity has been a fascinating subject of study for condensed matter physicists since its discovery almost a century ago. This new state of matter characterized by current flow with no dissipation and perfect diamagnetism was discovered by Kamerlingh Onnes in 1911. Despite intensive research, it eluded complete understanding for four decades until two different approaches provided a satisfying explanation of the phenomenon: one was the phenomenological theory of Ginzburg and Landau [1] and the other the microscopic theory of Bardeen, Cooper and Schrieffer (BCS) [2].

Ginzburg and Landau started from the Landau theory of phase transitions. They introduced a complex pseudo-wavefunction for the superconducting electrons as order parameter ψ and using a variational principle, they derived a differential equation similar to the Schrödinger equation for a free particle, but with a non-linear term. Their theory concentrated on superconducting electrons. The supercurrent was described by an expression similar to the quantum mechanical current for a particle with a charge e^* and mass m^*. They introduced a characteristic length, the coherence length ξ over which the order parameter can change without undue energy increase.

The BCS theory on the other hand described the superconductor on a microscopic level as a condensate of electrons pairs. They showed that the electron-phonon interaction caused the metallic ground state to be unstable to the formation of electron pairs, the Cooper pairs. These pairs of electrons in the ground state are separated from the excitations, quasiparticles, by an

energy gap Δ. The many-particle condensate wavefunction maintains phase coherence over macroscopic distances. Later, Gor'kov demonstrated that the Ginzburg-Landau theory is indeed a limit of the BCS theory close to the transition temperature (T_c) and that the order parameter ψ is directly proportional to the energy gap Δ.

In the mid-80s, the discovery of high temperature superconductivity by Bednorz and Müller opened a new era in the field. Complicated layered copper oxides, antiferromagnetic insulators in their native states, achieved extremely high transition temperatures into the superconducting state upon hole doping. Unexplained by the BCS theory, the microscopic mechanism of pairing in those materials is still a subject of open debate. Following that astonishing finding, more and more exotic compounds were synthesized and tested for superconductivity. Although hole-doped cuprates have kept the record for the highest transition temperatures by a comfortable margin, a large number of unconventional superconductors, i.e., superconductors that do not obey the BCS pairing mechanism have been discovered: examples are the heavy fermions, the organic superconductors, the borocarbides, and the ruthenates, including the object of the present study, Sr_2RuO_4. Discovered to be superconducting in 1994, it was the first confirmed triplet superconductor. Because it has broken time reversal symmetry and two degenerate order parameters, it has been postulated to have order parameter domains.

In this study, we present Josephson interferometry measurements of weak links made with Sr_2RuO_4 that show evidence for these domains. The technique of Josephson interferometry was developed 20 years ago and was used to determine unambiguously the pairing symmetry of the cuprate superconductors. When more than one phase is present across a superconducting Josephson junction, the interference is captured in the critical current mod-

ulation in an applied magnetic field. Josephson devices can be designed to exploit the phenomenon and give valuable information on the order parameter phase of unconventional superconductors, from which the pairing symmetry can be deduced.

This thesis is organized as follows: In the first chapter we introduce the material that we will be studying, Sr_2RuO_4, and present previous theoretical and experimental work that is most relevant to this study. A more complete overview can be found in [3]. In the second chapter, we present the method used to probe the system: Josephson interferometry. We discuss its theoretical foundation, the instances where it has been used as well as important factors that need to be taken into account when analyzing the data. In the third chapter, we talk about the experimental setup and details of the measurements. In the fourth and fifth chapters we present the experimental results of this work and we finish with a conclusion.

2 Superconductivity in Sr_2RuO_4

Sr_2RuO_4 is a material of the Ruddlesden-Popper series of ruthenium oxides given by $Sr_{n+1}Ru_nO_{3n+1}$, the only superconductor in the series. Its has a body centered tetragonal crystal structure of the type K_2NiF_4. Unlike most materials with the same crystal structure, it shows very little structural distortions and no transition to a different crystal structure at low temperature. The surface (ab-plane) undergoes a reconstruction to a ferromagnetic state when cleaved along the c-axis as observed by Scanning Tunneling Microscopy (STM) [4]. It is chemically very stable. The material was first synthesized in order to be used as a substrate for cuprates but was later found to be the first superconducting layered oxide without copper, with an unremarkable transition temperature of 1.5K. Because it is a good Fermi-liquid and isostructural to $La_{2-x}Ba_xCuO_4$ (see Fig.2.1), a high T_c superconductor, the stakes were high in trying to understand the superconductivity in the material: it provided the opportunity to study unconventional superconductivity originating from a well understood normal state. An additional similarity to the cuprates is the proximity to a Mott insulator, the isostructural and isoelectronic Sr_2FeO_4. Sr_2RuO_4 can be synthesized in fairly large single crystals of very high purity. Thin films made so far do not superconduct, presumably because of disorder.

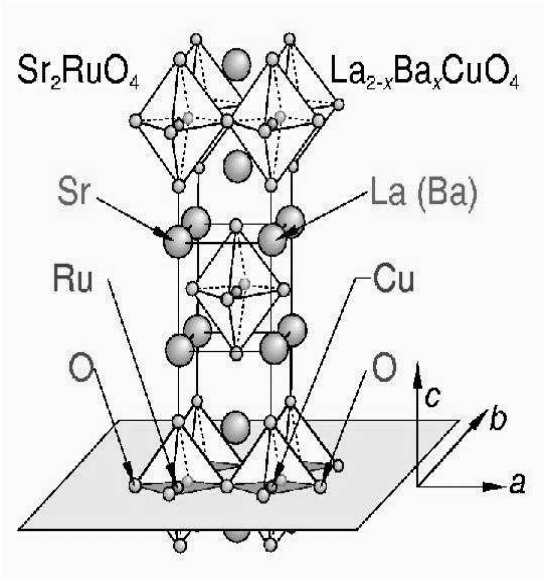

Figure 2.1 *Crystal structure of Sr_2RuO_4 and isostructural $La_{2-x}Ba_xCuO_4$. From [3].*

2.1 Normal state properties

Soon after the discovery of superconductivity in the material, Oguchi [5] calculated the band structure of the material in the local density approximation framework. He found three bands crossing the Fermi-surface, that were later labeled α, β and γ. The Fermi surface sheets are cylindrical; two are electron-like, β and γ, while the third, α, is hole-like.

The very high purity of the Sr_2RuO_4 single crystals made possible the measurement of quantum oscillations in the material [6]. They are oscillations of the resistivity or the magnetization as a function of the magnetic field, respectively called Shubnikov-de Haas and de Haas-van Alphen effects. They originate from the Landau quantization of the quasiparticle orbits leading to a cyclotron motion on each of the Fermi sheets. Since these oscillations decay exponentially with temperature and scattering, they can only be measured in materials with very long mean free path and, for superconductors, fairly low critical field. They carry a lot of information on the electronic structure of the material. The measurements essentially confirmed structure of the

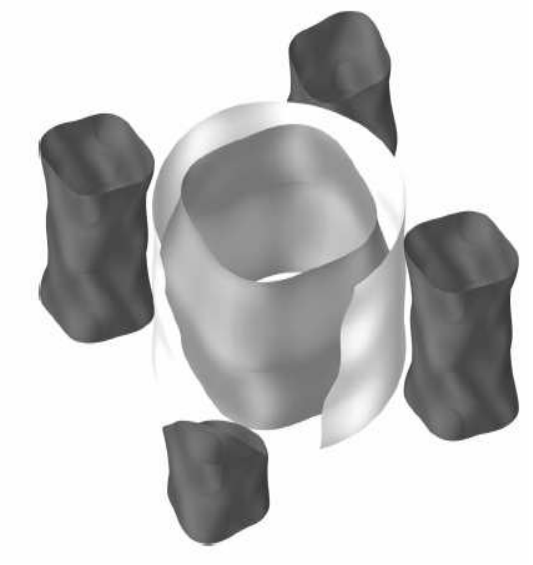

Figure 2.2 *Fermi surface of Sr_2RuO_4, as measured by quantum oscillations. From [3].*

calculated Fermi-surface although they revealed small modulations in the cross sectional area along the c-axis and they estimated an effective mass enhancement of 3.3 on the α sheet, 7 on the β sheet and 16 on the γ sheet [7]. A rendering of the Fermi surface is shown in Fig.2.2 .

The low temperature properties of the material are in good agreement with a two-dimensional Fermi-liquid. The electrical resistivity is highly anisotropic: the ratio of the in-plane to the c-axis resistivity ρ_{ab}/ρ_c varies from 400 to 4000. Below 20K, the two have a T^2 temperature dependence and their ratio becomes constant as predicted by Fermi-liquid theory. The c-axis resistivity first increases upon cooling, reaches a maximum at approximatively $130K$, and then decreases with temperature. That non-monotonic temperature dependence comes from a crossover from incoherent transport along the c-axis at high temperature to a fully three-dimensional transport

in the material at lower temperatures. A residual resistivity lower than $1\mu\Omega - cm$ is another indication of very high purity in the material. The specific heat can be fitted by a linear electronic term plus a cubic phonon term with a constant electronic coefficient below 15K. Calculations of the electronic coefficient of specific heat yield a value too small by a factor of 3 to 4, which is an indication of strong electron correlations that the local density approximation does not account for.

The static magnetic susceptibility is isotropic, a sign that it is not dominated by electrons but instead by the spin or Pauli term. Nuclear Magnetic Resonance (NMR) of ^{17}O and ^{101}Ru give evidence for ferromagnetic fluctuations [8] in the material, while inelastic neutron scattering measurements [9] have confirmed a theoretical prediction of incommensurate spin fluctuations at wave vector $(\pm 0.6\pi/a, \pm 0.6\pi/a, 0)$.

2.2 Superconducting state properties

When the superconductivity in Sr_2RuO_4 was discovered, the first step was to establish similarities to the cuprates since their crystal structures were similar. Nishizaki *et al.* [10] studied the dependence of the transition temperature on the oxygen partial pressure during high temperature annealing. They found a remarkable chemical stability: unlike in the cuprates, T_c did not depend on the annealing conditions. ^{101}Ru NMR and Nuclear Quadrupole Resonance (NQR) [11] experiments failed to find the Hebel-Slichter coherence peak, giving a hint to the unconventional superconductivity. But the most convincing proof came from a series of studies on the importance of non-magnetic impurities on the superconducting state in the material.

2.2.1 Sensitivity to impurities

As more crystals were synthesized, a large disparity in the transition temperatures of different batches was noticed. Since some sort of doping mechanism had been ruled out by the oxygen annealing experiment, one possible explanation was the presence of impurities. Magnetic impurities always suppress superconductivity because they act as Cooper pair breakers. Anderson's theorem [12] states that elastic scattering of Cooper pairs off non-magnetic impurities does not act as a pair breaker in conventional superconductors. An intuitive explanation of the theorem is that the scattering only does a mixing of states, averaging the Fermi velocity of the pairs. For an isotropic gap, the averaging has no effect on the size of the gap; for a gap isotropic in phase and anisotropic in magnitude, the so called anisotropic s-wave, the averaging changes the size of the gap, increasing it at the minimum points and decreasing it at maxima, but it does not destroy it all together. Since the magnitude of the gap is the average of two positive numbers, it remains finite. For unconventional order parameters that exhibit sign changes, the sum of the order parameter over the entire Fermi surface vanishes and hence the gap can be completely suppressed by non-magnetic impurities. The exact derivations can be found in the works of Anderson [12], Balian *et al.* [13] and Larkin [14].

Although theoretical predictions were made some time ago, experimental verification of the phenomenon was first done on Sr_2RuO_4. Mackenzie *et al.* ([15, 16]) measured the impurities in crystals with T_c varying from $20mK$ to $1.3K$. They used a high precision microprobe analysis to check for elements with atomic numbers between $15(Na)$ and $83(Bi)$ with a precision greater than 50 parts per millions. They found correlations between traces of silicon

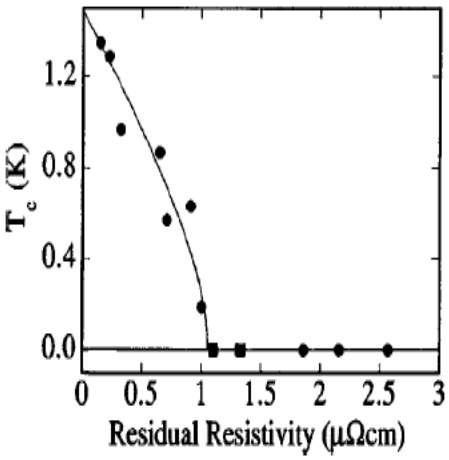

Figure 2.3 *Suppression of T_c in Sr_2RuO_4 as the residual resistivity increases. From [16].*

and aluminum, the residual resistivity of the samples, and their transition temperatures. They gave clear evidence that non-magnetic impurities suppress superconductivity in Sr_2RuO_4 and strong support to the possibility of unconventional superconductivity in the material. Their findings are summarized in (Fig.2.3). These results raised the question of how to interpret data from low T_c samples and emphasized the need for very high purity samples, making the quest easier by providing the residual resistivity as a measure of sample purity. They were able to deduce from their measurements the mean free path in the samples. The purest samples made today have mean free paths as long as $3\mu m$ and reach the highest predicted T_c of $1.5K$.

A subsequent study demonstrated that the same pair breaking effect by impurities could be achieved by introducing crystal defects through changes to growth conditions [17]. More studies of the effect on the upper critical field and isotope effect [18] showed good agreement with theoretical predictions of pair breaking in unconventional superconductors.

2.2.2 Fundamental parameters of the superconducting state

Because of the drastic effect of impurities and defects on the superconducting state, the early measurements of the superconducting parameters were not trusted until verified on high quality crystals with a T_c of at least $1.4K$. Akima *et al.* [19] determined the in-plane and out-of-plane resistivity in applied magnetic field of 0 to $7T$ on a crystal with a T_c of $1.49K$ and a residual resistivity of $0.47\mu\Omega - cm$. They covered a temperature range going from T_c down to $0.2K$. They found a similar temperature dependence of the resistivity in the normal state for low and high T_c crystals ($0.9K$ and $1.49K$). By extrapolating the measured upper critical field (H_{c2}) to $0K$, they deduced values for the in-plane and out-of-plane critical field of $\mu_0 H_{c2//ab}(0) = 1.5T$ and $\mu_0 H_{c2//c}(0) = 0.075T$. Using the Ginzburg-Landau formula for anisotropic superconductors, they could extrapolate coherence lengths to be $\xi_{ab}(0) = 660\mathring{A}$ and $\xi_c(0) = 33\mathring{A}$, with an anisotropy $\xi_{ab}(0)/\xi_c(0) = 20$. All three quantities were lower than the ones observed in the lower T_c crystal. To determine the Ginzburg-Landau parameter, they measured the low temperature specific heat and extracted from it the thermodynamic critical field $\mu_0 H_c(0) = 0.0194T$. That value was later revised from more precise measurements [20] to be $0.023T$ and the Ginzburg-Landau parameters deduced from it were $\kappa_{ab}(0) = 2.3$ and $\kappa_c(0) = 46$, which gave penetration depths values of $\lambda_{ab}(0) = 1520\mathring{A}$ and $\lambda_c(0) = 30000\mathring{A}$.

2.2.3 Symmetry of the superconducting order parameter

Superconductivity is a state of spontaneously broken symmetry. In conventional superconductors, the superconducting order parameter is the simplest possible: the only broken symmetry at the transition is the gauge symmetry and the Cooper pair orbital angular momentum is the lowest possible, $L = 0$. Unconventional superconductors are by definition superconductors that break additional symmetries. The additional symmetries that can be broken are the point group of the crystal lattice symmetry, the spin rotation symmetry group, and the Time-Reversal Symmetry (TRS) group. For any superconductor, the order parameter symmetry is a subgroup of the group of symmetries of the crystal. A complete list of allowed order parameters can be calculated from the crystal structure of the material [21]. Experimental results are then used to narrow the list and eventually find the correct order parameter. The symmetry of the order parameters is usually referred to as $s-$wave, $d-$wave, $p-$wave, ... corresponding to the orbital angular momentum states of the Cooper pairs. Since the electrons have to obey Fermi statistics, even orbital angular momentum states correspond to an antisymmetric pairing of the spins, i.e., spin singlet, while odd orbital pairing corresponds to symmetric spin triplet pairing. Strictly speaking, these names shouldn't apply in the presence of a crystal field since the angular momentum is not a good quantum number: Cooper pairs contain a mixture of angular momentum states. The notation can still be valid if interpreted in terms of the symmetry of the orbital wave function corresponding to the state and the spherical harmonics that describe it [21].

For unconventional superconductors, the broken symmetries dictate the

pairing state: spin singlet states, such as the $d-$wave pairing state, break gauge and lattice point group symmetries while triplet states also break both the spin rotation and TRS. Note that for singlet states, TRS can still be broken by complex order parameters, states for which the order parameter has more than one component such as $s + id$ pairing state. The second component of the order parameter appears below T_c either by another phase transition, as is the case in crystals of tetragonal symmetry, or gradually, as it could be the case for cubic systems [22]. If they are not complex, order parameters of unconventional superconductors have a number of line nodes equal to the corresponding "angular momentum" state: one for $p-$wave, two for $d-$wave, ...

Each of these broken symmetries is accompanied by changes in physical properties that can be identified by experiments. Following Annett's classification [22], let's present the experiments in five classes that distinguish what type of information they provide on the order parameter.

The first class include experiments showing evidence of more than one phase transition. They differentiate $s-$wave from other pairing symmetries: $s-$wave pairing corresponds to a one-dimensional irreducible representation while a multi-component order parameter is always unconventional. They are observed through derivatives of the free energy such as a double peak in the specific heat.

The second class of experiments are the so-called phase sensitive techniques that measure the macroscopic order parameter symmetry, using the Josephson effect. They can map out the anisotropy of the phase of the order parameter. The two principal experiments in that class are Josephson interferometry and Scanning SQUID Microscopy (SSM). We will talk more about the interferometry measurements in the next chapter.

The third class distinguishes spin singlet from spin triplet pairing by measuring the electronic spin susceptibility of the material. In singlet superconductors, that quantity goes to zero below T_c since the pairs have no net spin, but in triplet superconductors, it can remain non-zero at the lowest temperatures. An example of this type of measurement is the Knight shift which measures the shift in NMR frequency caused by the electronic spin susceptibility.

The fourth class include experiments that measure whether or not the energy gap has a zero average over the Fermi surface. The average is non-zero only if the order parameter has a non-zero $s-$wave component. Experiments belonging to this class include sensitivity to non-magnetic impurities and the presence of a coherence peak at the transition in the temperature dependence of the NMR relaxation rate or the ultrasound attenuation.

The fifth and last class is that of experiments that determine the presence of nodes in the gap function. In this class are all the experiments that measure the density of states at low temperatures. The temperature dependence of the specific heat, penetration depth, NMR or NQR relaxation rate,... is exponential for s-wave superconductors but follows a power law in the presence of nodes: T^2 for line nodes and T^3 for point nodes. Some of these techniques have been perfected to give information on the directionality of the nodes, for example Angle Resolved Photo-Emission Spectroscopy (ARPES), specific heat and thermal conduction in magnetic field and ultrasound attenuation.

An important addition to that classification would be experiments probing broken TRS. They include MUon Spin Relaxation (μSR) that measures a spontaneous magnetic moment below T_c, magnetic field distribution of the vortex lattice as can be measured by neutron scattering, and the high resolution polar Kerr effect that measures an antisymmetric contribution to the

real and imaginary parts of the dielectric tensor.

The interpretation of these experiments is not always straightforward because, in many cases, effects similar to those of a broken symmetry can have a different origin in a material. It usually takes many of them pointing to the same conclusions before the exact order parameter can be established. The phase sensitive techniques in the second class are especially nice because they provide a direct measurement of the phase of the order parameter.

2.2.4 $p-$wave superconductivity

For superconductors with spin triplet pairing, there need to be three order parameters, corresponding to the three states of the spin triplet. They are expressed in terms of the gap function $\Delta(\mathbf{k})$ that can be written as a 2×2 matrix in the form

$$\Delta(\mathbf{k}) = \begin{bmatrix} \Delta_{\uparrow\uparrow} & \Delta_{\uparrow\downarrow} \\ \Delta_{\downarrow\uparrow} & \Delta_{\downarrow\downarrow} \end{bmatrix} \tag{2.1}$$

where $\mathbf{k}$ is a unit vector specifying a direction in momentum space and the elements of the matrix are the spin states of the electrons constituting the Cooper pair. In the triplet case, $\Delta_{\uparrow\downarrow} = \Delta_{\downarrow\uparrow} = \Delta_0$. An elegant equivalent formalism is that of the $\mathbf{d}$-vector: the matrix is replaced by a three component complex vector $\mathbf{d}(\mathbf{k}) = [d_x(\mathbf{k}), d_y(\mathbf{k}), d_z(\mathbf{k})]$ with

$$\Delta(\mathbf{k}) = \begin{pmatrix} \Delta_{\uparrow\uparrow} & \Delta_0 \\ \Delta_0 & \Delta_{\downarrow\downarrow} \end{pmatrix} = \begin{pmatrix} -d_x + id_y & d_z \\ d_z & d_x + id_y \end{pmatrix}. \tag{2.2}$$

Besides having a compact form analogous to the gap function of singlet superconductors (a complex vector instead of a complex scalar), it has the advantage of transforming like a vector under a rotation of spins.

The state vector of a triplet superconductor can then be expressed as

$$|\psi\rangle = \Delta_{\uparrow\uparrow}|\uparrow\uparrow\rangle + \Delta_{\downarrow\downarrow}|\downarrow\downarrow\rangle + \Delta_0(|\uparrow\downarrow\rangle + |\downarrow\uparrow\rangle), \tag{2.3}$$

where the bases $|\uparrow\uparrow\rangle$, $|\downarrow\downarrow\rangle$ and $(1/\sqrt{2})(|\uparrow\downarrow\rangle + |\downarrow\uparrow\rangle)$ correspond to the spin projections $S_z = 1$, -1 and 0, respectively. If the bases are changed to $\mathbf{x}$, $\mathbf{y}$ and $\mathbf{z}$ defined as

$$\mathbf{x} = |S_x = 0\rangle = \frac{1}{\sqrt{2}}(-|\uparrow\uparrow\rangle + |\downarrow\downarrow\rangle), \tag{2.4}$$

$$\mathbf{y} = |S_y = 0\rangle = \frac{1}{\sqrt{2}}(|\uparrow\uparrow\rangle + |\downarrow\downarrow\rangle), \tag{2.5}$$

$$\mathbf{z} = |S_z = 0\rangle = \frac{1}{\sqrt{2}}(|\uparrow\downarrow\rangle + |\downarrow\uparrow\rangle), \tag{2.6}$$

then the state can be written as

$$|\psi\rangle = \sqrt{2}(d_x\mathbf{x} + d_y\mathbf{y} + d_z\mathbf{z}). \tag{2.7}$$

The quasiparticle excitation energy spectrum is then given by

$$E_k = \sqrt{\epsilon_k^2 + \mathbf{d}\cdot\mathbf{d}^* \pm |\,\mathbf{d}\times\mathbf{d}^*\,|}, \tag{2.8}$$

where E_k is the energy of the quasiparticle and ϵ_k is the excitation energy referenced to the chemical potential.

For a unitary state, $|\mathbf{d}\times\mathbf{d}^*| = 0$ and $\mathbf{d}\cdot\mathbf{d}^*$ can be identified with the square of the energy gap $|\Delta(\mathbf{k})|^2$. All the electrons are paired and the order parameter $\mathbf{d}(\mathbf{k})$ has a physical meaning: the magnitude is proportional to the energy gap and the direction is normal to the plane in which the electrons of momentum $(-\mathbf{k}, \mathbf{k})$ are equal spin paired. A nonunitary state has

two distinct energy gaps, and one of them can completely vanish, leading to a superconducting state with finite excitations, even at $T = 0$. Nonunitary states break TRS: the structure of their pair correlations is different for up and down spins in different directions of $\mathbf{k}$. They are associated with a magnetic moment. Although largely screened due to the Meissner effect, a small fraction of the magnetization survives at sites where the order parameter is suppressed: at impurities or defects sites or at the surface.

2.2.5 Experimental investigation of the order parameter symmetry

The very first evidence of unconventional superconductivity in Sr_2RuO_4 was, as presented earlier, the sensitivity of the superconductivity to non-magnetic impurities. The experimental results ruled out both isotropic and anisotropic $s-$wave order parameters, making it clear that the material was an unconventional superconductor.

The first, and to date the strongest, experimental evidence for triplet pairing came from the measurement of the spin susceptibility in the superconducting state by NMR. The spin susceptibility in superconductors is hard to measure directly because of Meissner screening. It is typically measured indirectly through the Knight shift: the difference between the NMR resonance frequency of a nucleus when it is in a metal or a superconductor from when it is in an insulator. The Knight shift has an orbital part due to diamagnetism of the bound and free electrons and a spin part due to the Pauli paramagnetism of the conduction electrons. In singlet superconductors, it should drop steadily below T_c and go to zero exponentially at low temperatures [23]. Ishida and co-worker performed ^{17}O [24] and ^{101}Ru [25]

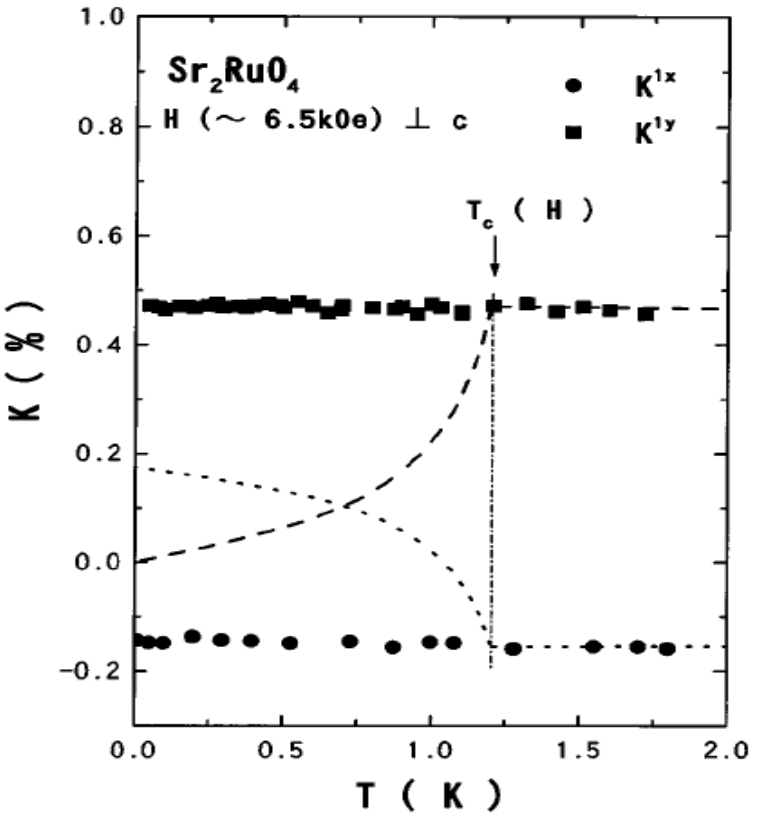

Figure 2.4 *The electronic spin susceptibility measured by the Knight shift in NMR frequency in Sr_2RuO_4 remains constant through the superconducting transition for both oxygen sites K^{1x} and K^{1y} (solid symbols). The dashed and dotted lines represent the expected spin susceptibility for singlet superconductors. From [26].*

NMR for a field perpendicular to the $c-$axis and found that the spin part of the Knight shift is completely unchanged as the system goes through the superconducting transition (Fig.2.4), strong evidence for triplet pairing in the material.

This conclusion was emphasized by another experiment in favor of triplet pairing: polarized neutron scattering used to measure the spin susceptibility [27]. An applied magnetic field induces a magnetization density in the periodic crystal with spatial Fourier components at reciprocal lattice vectors. Through a diffraction experiment, the spatially varying components of the magnetization can be measured, even in the superconducting state. They

found a constant spin susceptibility above and below T_c in the material. Another experiment has used Josephson interferometry to show evidence for odd symmetry pairing in Sr_2RuO_4 [28], which is also direct evidence for spin triplet pairing. We will discuss it in more details in the next chapter.

One manifestation of broken TRS in the material is a spontaneous magnetization that appears below T_c. Because of Meissner screening, the magnetization is only observable on very local scales, at points where the screening is imperfect, such as crystal defects or impurities. One of the best probes for the phenomena is μSR, where polarized muons are implanted in the material, precess by reacting with the local spin at the implantation site, and decay by emitting a positron preferentially in the direction of the muon spin at the time of the decay. The study by Luke *et al.* [26] shows spontaneous magnetization at T_c with a gaussian distribution of the relaxation rate, a sign of a broad distribution of magnetic fields arising from a dilute distribution of currents (Fig.2.5).

To confirm that the increased relaxation rate was caused by broken TRS and not by a magnetic phase accidentally onsetting at the superconducting transition temperature, they measured samples of various T_c and found that the spontaneous magnetization always coincided with the superconductivity. A subsequent small angle neutron scattering study [29] showed that the vortex lattice in the material was square at all field values, which is consistent with a TRS-breaking state and a two components order parameter.

Recently, a measurement of the polar Kerr effect in the material provided additional evidence for broken TRS [30]. It measured the existence of an antisymmetric component to the real and imaginary parts of the frequency dependent dielectric tensor, which is only present when TRS is broken. They find a polar Kerr effect that appears at T_c and whose magnitude increases as

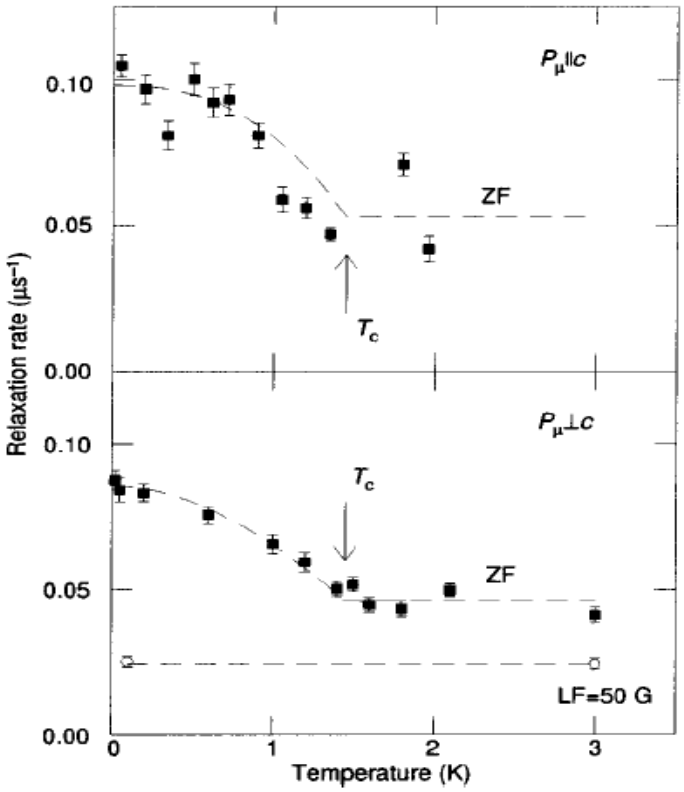

Figure 2.5 *Increase in the relaxation rate appearing at T_c for implanted muons polarized in-plane (top) and out-of-plane (bottom). It is a manifestation of spontaneous magnetization. From [26].*

the temperature is lowered, tracking the superconducting order parameter in the material.

Note that the broken TRS at T_c provides indirect evidence for triplet pairing since symmetry considerations require that a singlet order parameter in a tetragonal crystal can only break TRS at an additional transition below T_c. Such a transition is not observed in Sr_2RuO_4.

All of these measurements agree on important facts in the determination of the order parameter of Sr_2RuO_4: the electrons are paired in a spin triplet state, which implies that the orbital part is of odd parity, and TRS is broken at the transition. Of all the triplet order parameters allowed by symmetry, the favored one has the lowest orbital angular momentum, i.e., $p-$wave order parameter, and is unitary [3]. The $\hat{\mathbf{z}}(p_x \pm ip_y)$ order parameter was proposed [31] before any of these experiments were performed by comparison of the normal state properties of Sr_2RuO_4 to those of superfluid helium. We will talk more about the properties associated with that order parameter in the next section.

A number of measurements have shown evidence for a residual density of states at low temperature [3]. They include measurements of the specific heat, penetration depth, nuclear relaxation rate in NMR and NQR, and thermal conductivity. This is seemingly in contradiction with the order parameter predicted above, which corresponds to an energy gap isotropic in magnitude. Directional probes, which can locate the direction of nodes, have yielded contradictory results. Thermal conductivity in applied magnetic fields and ultrasonic attenuation failed to resolve any in-plane anisotropy. Horizontal line nodes were then postulated. It is only recently that detailed measurement of the field orientation dependence of the specific heat [32] resolved a 4-fold anisotropy in the *ab*-plane. At present, the question is whether the

observed modulations are caused by nodes, where the phase of the order parameter changes sign from one lobe to another, by zeroes where the magnitude vanishes but the phase doesn't change sign, or by very deep but finite minima in the gap function. A favored explanation is that of Orbital Dependent Superconductivity (ODS) [33]. In this scenario, only one of the three Fermi sheets, γ, is responsible for the superconductivity while the other two, α and β, are passive bands. The γ sheet is believed to have four vertical lines of deep minima while the α and β would have line nodes.

2.2.6 Description of the $p_x \pm ip_y$ order parameter

This order parameter is represented by the **d**-vector

$$\mathbf{d} = \Delta_0 \hat{\mathbf{z}}(k_x \pm ik_y) = \Delta_0 \begin{bmatrix} 0 \\ 0 \\ k_x \pm ik_y \end{bmatrix}. \tag{2.9}$$

It is the same **d**-vector as for the A phase of superfluid Helium-3. It has an orbital angular momentum $L = 1$. Assuming that the presence of spin-orbit scattering locks the the z direction of the spin wave function on the c axis of the crystal, the **d**-vector can be expressed in terms of spherical harmonics as

$$Y_{1\pm1} = \left(\frac{3}{8}\pi\right)^{1/2} \sin\theta \exp(\pm i\phi) = \left(\frac{3}{8}\pi\right)^{1/2} (k_x \pm ik_y). \tag{2.10}$$

Since $L_z = \pm 1$, the Cooper pairs orbital motion in a given domain is in the xy-plane with clockwise and counterclockwise rotation leading to broken TRS. The spins lie in the xy-plane and are paired in an $S = 1$ state in an equally weighted superposition of $|\uparrow\uparrow\rangle$ and $|\downarrow\downarrow\rangle$ states for any quantization axis within the plane.

For a perfectly cylindrical Fermi surface, the energy gap is isotropic and two dimensional, with its phase continuously changing with angle to satisfy odd parity. If the Fermi surface cross-section is not circular, the gap is not isotropic and the gap functions should be modified to reflect the lattice symmetry.

2.2.7 Order parameter domains in Sr_2RuO_4

The broken TRS in the material yields interesting physics. Volovik and Gor'kov ([34], [35]) have classified states with broken TRS depending on the internal angular momentum of Cooper pairs: "ferromagnetic" states have either a finite angular momentum or, for non-unitary states, finite spin moment, while "antiferromagnetic" states have no net moments. The order parameter of Sr_2RuO_4 is, according to that classification, of the ferromagnetic type: even in the ground state, a current should flow along the surface of the material. To satisfy the Meissner effect, a screening current flows within a penetration depth to cancel the field caused by the ferromagnetic current in the bulk of the material so that there is no net magnetization in the bulk, but there will still be a magnetic moment at the surface of the material as well as at sites with a suppressed order parameter such as defects and impurities. To offset the cost of magnetic energy, the discrete degeneracy of the order parameter allows for the formation of order parameter domains, similar to those in ferromagnetic materials [35]. Since the domain walls are energetically costly, they will get pinned at defects or impurities sites. The different domains are called chiral domains, named after the two chiralities associated with the two degenerate order parameters $p_x + ip_y$ and $p_x - ip_y$.

A number of theoretical studies on domain-related physics in superconductors with broken TRS have been done. Sigrist *et al.* [36] have studied low

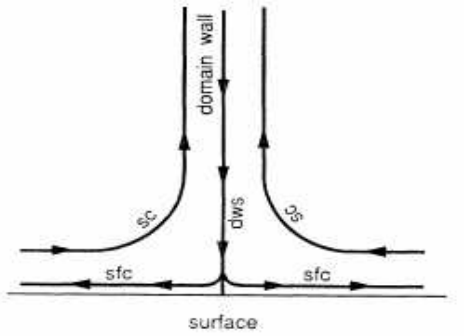

Figure 2.6 *Current flow pattern at the intersection of a domain wall and a surface. sc is the screening current, sfc is the surface current and dws is the current flowing in the domain wall. From [36].*

magnetic field response of complex superconductors by solving the Ginzburg-Landau equations and found that there is no current through the domain wall but there is a spontaneous current centered in the wall and flowing along it. They also found that vortices in domain walls could be distorted by a Lorentz force caused by the currents and that a single domain superconductor would have a finite net magnetization concentrated towards the surface. They also calculated what happens when a domain wall intersects a surface. The simplest current distribution that they found is given in Fig.2.6.

Another calculation involved quasi-particle states at the domain wall which, using the semi-classical approach [37], found that domain walls are in many aspects similar to surfaces. The component of the order parameter perpendicular to the normal of the wall is suppressed while the one parallel to the normal is enhanced. They found two types of domain walls: one where the suppressed order parameter component vanishes in the center of the wall and another that introduces a phase twist so that both components have a finite modulus everywhere. They also found a tiny gap in the local density of states in the center of one of the domain walls. They did emphasize that their results were only valid for a cylindrical Fermi surface and the real properties of the material could be different.

Although there is no unequivocal experimental observation of order parameter domains reported so far, there are measurements whose only proposed interpretation involves domains. One example is the work of Mota *et al.* who measured the rate of vortex creep dynamics in three superconductors with broken TRS: UPt_3, $U_{1-x}Th_xBe_{13}$ and Sr_2RuO_4 [38, 39, 40]. They found unusually high pinning in all three compounds at sufficiently low temperature. The two heavy fermions UPt_3 and $U_{1-x}Th_xBe_{13}$ have two distinct superconducting transitions. Below the lower transition temperature in those two materials and below $\sim 50mK$ in Sr_2RuO_4, the rate of vortex creep drops essentially to zero for periods of times longer than $10^5 s$. This requires a highly unusual pinning mechanism and the only explanation offered to date involves domain walls. Sigrist and Agterberg [41] explained these results in terms of fence-like structures that would stop the vortices from escaping the superconductor. These structures originate from the fact that on a domain wall, a vortex with integer flux quantum can degenerate into two or more vortices with fractional flux quantization. Since these vortices cannot move away from the wall, they become very efficient barriers to vortex motion. Domain walls have also been used to explain the ultrasound attenuation in UPt_3 [21] and vortex coalescence in Sr_2RuO_4 [42].

3 Josephson interferometry as a phase sensitive probe of order parameter symmetry

3.1 Josephson effects

Josephson effects are phenomena that occur in weak links, i.e., two superconductors decoupled enough to behave differently than the bulk superconductor but still preserve phase coherence between them. The weak link can be depicted by two superconductors L and R separated by a barrier sized to let the tails of their wave functions overlap (See Fig.3.1). There is a finite probability of Cooper pairs tunneling from one superconducting bank to the other. The phase difference across a weak link is different from that of the bulk because it is 2π periodic: after a 2π increase in the phase, the junction returns to its original state. Although the first derivation by B.D. Josephson in 1962 was for Superconductor/Insulator/Superconductor (SIS) structures, also known as tunnel junctions, the basic predictions are valid for a variety of devices, including Superconductor/Normal metal/Superconductor (SNS)devices and a superconductor with a very short and narrow constriction (ScS). These pre-

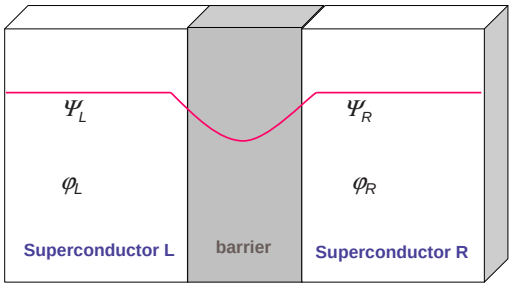

Figure 3.1 *Weak link between two superconductors L and R with respective order parameters Ψ_L and Ψ_R and phases φ_L and φ_R.*

dictions consist of two effects: the dc Josephson effect and the ac Josephson effect. They are derived in detail in a number of books (e.g. [23, 43, 44]).

The dc Josephson effect specifies the dc current flowing across the link as

$$I_s = I_J \sin \phi \tag{3.1}$$

where I_s is the current across the link, I_J is the Josephson critical current defined as the maximum supercurrent that can flow across the junction, and ϕ is the gauge invariant phase difference

$$\phi = \Delta\varphi - (\frac{2\pi}{\Phi_0} \int \mathbf{A}.ds) \tag{3.2}$$

between the two banks of the junction. A phase gradient across the junction causes current to flow through it. Here, $\mathbf{A}$ is a vector potential and $\Phi_0 = hc/2e = 2.07 \times 10^{-7} G - cm^2$.

The ac Josephson effect describes the behavior of the junction when a voltage is applied across it

$$d\phi/dt = 2eV/\hbar; \tag{3.3}$$

an alternating current of amplitude I_J and frequency $2eV/\hbar$ is present in the junction.

The Josephson coupling energy E_J in the junction can be obtained by integrating the electrical work done by a current source I_s in changing the phase

$$\int I_s V dt = \int I_s(\hbar/2e) d\phi. \tag{3.4}$$

It is given by

$$F = C - E_J \cos\phi, \tag{3.5}$$

where C is a constant and

$$E_J = (\hbar I_J / 2e). \tag{3.6}$$

The critical current is a measure of the coupling between the two superconductors. It depends on the junction area, the material and size of the barrier.

When the current through the junction is ramped to exceed the critical current, a normal, dissipative current flows in the junction in addition to the supercurrent and a voltage develops across it. The current is a non-linear function of the voltage. The junction can be modeled as a resistor in parallel with the junction in the Resistively Shunted Junction (RSJ) model. Across a Josephson junction, the phase of the order parameter can "slip" by 2π. It is as if a vortex singularity is entering the junction through one end, moving across the junction as the phase increases from 0 to 2π and exiting through the other end when the phase reaches 2π.

3.2 Josephson effect in the presence of a magnetic field

The description of Josephson junctions in magnetic field presented here closely follows the derivation in [44]. If a magnetic field H is applied to a junction along the $y-$ direction, as depicted on Fig.3.2, then the gauge invariant phase

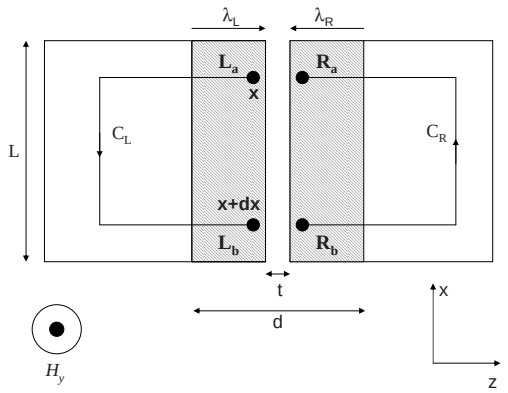

Figure 3.2 *Geometry of a Josephson junction in a magnetic field. $C_L(C_R)$ is the integration contour used to derive the magnetic field dependence of the phase difference φ. The field H_y is in the y direction. λ_L (λ_R) is the magnetic penetration depth on the left (right) superconductor and t is the barrier thickness.*

gradient along the barrier is given by

$$\nabla\varphi_{L,R} = \frac{2e}{\hbar c}\left(\frac{mc}{2e^2\rho}\mathbf{J}_S + \mathbf{A}\right). \tag{3.7}$$

$\mathbf{J}_S$ is the screening current density. By integrating along the contours C_L and C_R between x and $x + dx$ (see Fig.3.2) we get:

$$\varphi_{Ra}(x) - \varphi_{Rb}(x + dx) = \frac{2e}{\hbar c}\int_{C_R}\left(\mathbf{A} + \frac{mc}{2e^2\rho}\mathbf{J_S}\right)\cdot\mathbf{dl} \tag{3.8}$$

and

$$\varphi_{Lb}(x + dx) - \varphi_{La}(x) = \frac{2e}{\hbar c}\int_{C_L}\left(\mathbf{A} + \frac{mc}{2e^2\rho}\mathbf{J_S}\right)\cdot\mathbf{dl}. \tag{3.9}$$

If the superconductor is wider than the magnetic penetration depth on each side of the junction, the contours C_L and C_R can be outside the region where the field penetrates (shaded in Fig.3.2) and the supercurrent density vanishes on most of the integration path. If the integration path is chosen to be perpendicular to $\mathbf{J_S}$ in the shaded region, the second term in the two

integrals above disappear and we have

$$\varphi(x+dx)-\varphi(x)=[\varphi_{Lb}(x+dx)-\varphi_{Rb}(x+dx)]-[\varphi_{La}(x)-\varphi_{Ra}(x)] \tag{3.10}$$

and

$$\varphi(x+dx)-\varphi(x)=\frac{2e}{\hbar c}\left[\int_{C_L}\mathbf{A}\cdot\mathbf{dl}+\int_{C_R}\mathbf{A}\cdot\mathbf{dl}\right]. \tag{3.11}$$

Using the previously defined gauge invariant phase difference ϕ, we get

$$\phi(x+dx)-\phi(x)=\frac{2e}{\hbar c}\oint\mathbf{A}\cdot\mathbf{dl}. \tag{3.12}$$

Since

$$\nabla\times\mathbf{A}=\mathbf{H}, \tag{3.13}$$

then

$$\oint\mathbf{A}\cdot\mathbf{dl}=H_y(\lambda_L+\lambda_R+t)dx \tag{3.14}$$

and in differential terms

$$\frac{d\phi}{dx}=\frac{2e}{\hbar c}(\lambda_L+\lambda_R+t)H_y \tag{3.15}$$

where λ_L and λ_R are the penetration depths in the two superconductors and t is the barrier thickness. After integration, we have

$$\phi(x)=\frac{2e}{\hbar c}dH_yx+\phi_0 \tag{3.16}$$

where $d=(\lambda_L+\lambda_R+t)$ is the magnetic penetration depth. The critical current density in the presence of a magnetic field is then

$$J(x)=J_c\sin\left(\frac{2e}{\hbar c}dH_yx+\varphi_0\right), \tag{3.17}$$

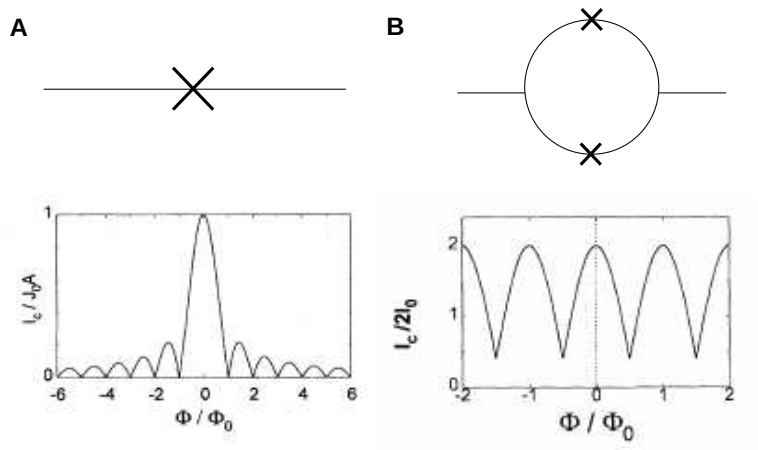

Figure 3.3 *Modulation of the critical current in an applied magnetic field for (A) a Josephson junction; (B) a SQUID with a finite inductance.*

where J_c is the critical current density. The magnetic field modulates the critical current. For a rectangular junction, modulations from a uniform field follow a Fraunhöfer pattern (see Fig.3.3(A)), as for diffraction of light through a slit. Defining the flux through the junction as $\Phi = HLd$, the critical current can be given as a function of the magnetic flux as

$$I_c(H) = I_c(0) \left| \frac{\sin\left(\pi \frac{\Phi}{\Phi_0}\right)}{\pi \frac{\Phi}{\Phi_0}} \right| \tag{3.18}$$

Notice that the calculation presented above assumes the "small junction limit", in which the junction is small enough that the magnetic fields produced by the current are negligible. For larger junctions, or equivalently if much larger currents flow through the same size junction, the self-field effects caused by the currents induce screening currents and the Josephson currents are confined to the edges of the junctions. That happens when the junction size becomes larger than the Josephson penetration depth, defined as

$$\lambda_J = \left(\frac{\hbar c^2}{8\pi e d J_c} \right)^{1/2}. \tag{3.19}$$

λ_J depends on J_c and for conventional superconductors is typically of the order of hundreds of microns.

If two Josephson junctions are connected in parallel, they form a dc Superconductor QUantum Interference Device (SQUID). In an applied magnetic field, the SQUID's critical current modulates following a two slit interference pattern. For small loop inductance, it is given by the expression

$$I_c(\Phi) = 2I_0 \left|\cos\left[\pi\frac{\Phi}{\Phi_0}\right]\right| \tag{3.20}$$

where Φ is the magnetic flux through the loop. A schematic and interference pattern of a SQUID is given in Fig.3.3(B). This is for a SQUID with finite loop inductance: the critical current does not modulate all the way to zero.

3.3 Josephson interferometry for phase sensitive measurements in unconventional superconductors

Josephson interferometry aims to map out the phase of an unconventional superconducting order parameter through measurements of interference patterns of bimetallic Josephson devices, junctions or SQUIDs, made with the unconventional superconductor and a conventional superconductor. It is based on two principles [45]. First, the interference or diffraction pattern carries information on the phase differences between different parts of the junction and hence if the phase information from one of the electrodes is known, the phase information from the unconventional material can be deduced. Second, Josephson tunneling is highly directional: in each junction,

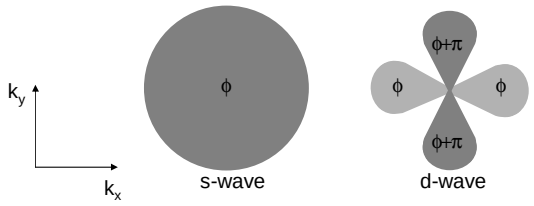

Figure 3.4 *k-space representation of s-wave and d-wave order parameters. The s-wave order parameter is isotropic while the d-wave order parameter has a phase difference of π between the k_x and k_y direction.*

the Cooper pairs tunneling probability is highly peaked for forward tunneling and the unconventional superconductor is probed in the direction perpendicular to the junction interface. In order to better explain the method, let's describe the experiments that pioneered the field.

3.3.1 SQUID interferometry experiments in cuprates

The fundamental question to answer was whether the order parameter of the high temperature cuprate superconductors had an s-wave pairing symmetry, i.e., an isotropic phase in k-space or if it had a d-wave pairing symmetry, i.e., a phase difference of π in orthogonal directions in k-space (see Fig 3.4). The first Josephson interferometry experiment to measure the phase anisotropy on an unconventional superconductor was the dc SQUID experiment on $YBa_2Cu_3O_{7-x}(YBCO)$ [46].

The device they used was a bimetallic ring of a single crystal of $YBCO$ with Josephson junctions on two orthogonal sides of the crystal. The loop was completed by a Pb thin film (see Fig.3.5). For a completely symmetric SQUID with equal critical currents in both junctions and vanishingly small loop inductance, the critical current of such a device is given by

$$I_c(\Phi) = 2I_0 \left|\cos\left[\pi\frac{\Phi}{\Phi_0} + \delta_{ab}\right]\right| \tag{3.21}$$

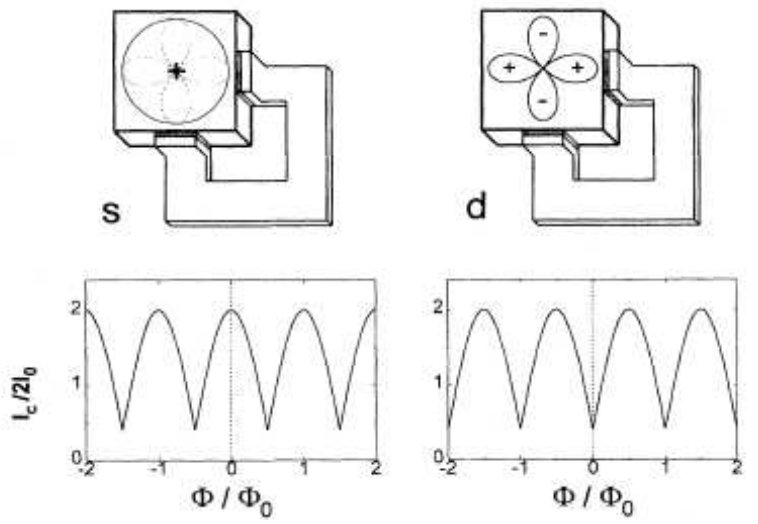

Figure 3.5 *Schematic of a SQUID interferometer for s-wave and d-wave order parameter (top) and corresponding interference patterns (bottom). From [45].*

which is a generalized version of Eq.3.20 where the possibility of an intrinsic phase shift inside the crystal δ_{ab} is accounted for. The interference patterns of these devices are different depending on the value of the intrinsic phase shift δ_{ab} (See Fig.3.5). If there is no phase shift ($\delta_{ab} = 0$), the critical current is maximum for no applied field. For a phase shift $\delta_{ab} = \pi$, the critical current is minimum at zero field because of the destructive phase interference in the two junctions and the critical current maximum with $\Phi_0/2$ flux in the junction. For a finite loop inductance L, the screening parameter $\beta = 2LI_0/\Phi_0$ is finite. Hence, circulating currents generate a flux contribution to the loop and the modulation depth of the critical current is reduced.

Although from a theoretical perspective it might seem trivial to distinguish between the two cases ($\delta_{ab} = 0$ and $\delta_{ab} = \pi$), there are a number of issues that might complicate the interpretation of the experimental results [45]. Asymmetry in the SQUID, caused either by different critical currents for the two junctions or by asymmetry in the two arms of the SQUID can cause patterns to suppress, skew or shift. A shift would cause the biggest

problem since it could possibly mimic a phase difference. It can come from three sources: a finite loop inductance, an asymmetric inductance in the SQUID arms and residual magnetic fields. The residual fields are taken care of by very careful magnetic shielding of the experimental setup that reduces the residual field to the point where it causes a shift much smaller than half a flux quantum. Typically this is achieved by using high permeability mu-metal and superconductor shielding. Trapped magnetic flux near the SQUID is another problem. Depending on where it is trapped, a vortex can generate a local field that creates a phase shift that is indistinguishable from an intrinsic symmetry induced phase shift. The best way to handle the problem is to cool the SQUID many times in order to determine the most probable state, normally the one with no trapped flux. One issue that was raised as a potential problem was that the corner of the crystal inside the SQUID loop could create a singularity in the supercurrent flow or a high probability site for vortex trapping but there was no evidence of either of these effects in the experiment [47].

In the actual measurement, edge SQUIDs were used as control samples since they share all complicating factors with corner SQUIDs but they do not have the intrinsic phase shift between junctions. Because the critical current modulations were very small, they measured the modulations in the dynamic resistance at a constant current bias. They detected noticeable effects of the asymmetric branching of the critical current through the shift in the patterns as the current bias was changed (see Fig.3.6(A)).

In order to deduce the intrinsic phase shift in the junctions, they reduced the bias current until the effect of the asymmetry was negligible and they extrapolated the results to the zero current limit. As a result, they could differentiate between edge SQUIDs, which always showed no phase differ-

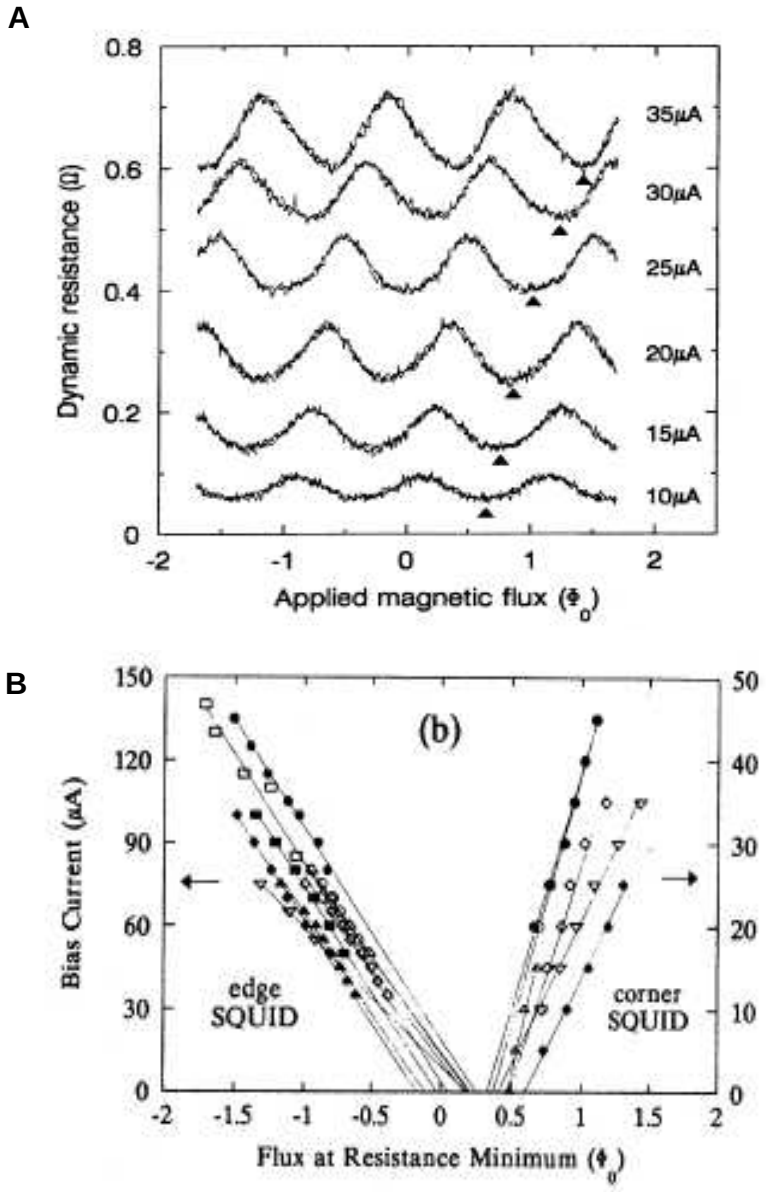

Figure 3.6 *Results of corner SQUID experiment. (A) Modulations of the critical current with applied field in a corner SQUID for different values of the bias current. The position of the minimum indicated by arrows changes with the bias current, proof of asymmetries in the device and tends to* $\Phi_0/2$ *as the bias current goes to 0. (B) Comparison of corner and edge SQUIDs on the same crystal cooled down many times, with an extrapolation of the phase shift for zero bias current (no asymmetry effects). The minimum extrapolates to 0 for the edge SQUID and to* $\Phi_0/2$ *for the corner SQUID. From [46].*

ence between the two junctions, and corner SQUIDs, which showed a phase difference of π. To account for trapped flux, they measured a corner and edge SQUIDs on the same crystal for many cooling cycles; the results are presented on Fig.3.6(B). The positions of the minima are distributed around 0 for edge SQUIDs and around $\Phi_0/2$ for corner SQUIDs.

3.3.2 Single junction interferometry in cuprates

An alternative method for determining the phase difference between tunneling directions is the study of modulations of critical current of single Josephson junctions. The method is an improvement over SQUID interferometry. Because there is no loop, any problem coming from loop inductance or asymmetry is avoided. This experiment gave the most convincing demonstration of the sign change in the order parameter inherent to $YBCO$ crystals.

The concepts behind the experiment are mostly the same as for the SQUID interferometry experiment. The testing device is a bimetallic Josephson junction fabricated at the corner of $YBCO$ single crystals as shown in Fig.3.7(C). The junctions have a Au barrier and Pb counterelectrodes. The control device is an edge junction, shown in Fig.3.7(A).

In this geometry, as in the corner SQUID, part of the tunneling is along the crystal's a-axis and part is along the b-axis. For an s-wave order parameter, there is no phase difference between orthogonal directions and the diffraction pattern is still given by Eq.3.18 (Fig.3.7(B)). For a d-wave order parameter, the π phase difference between the tunneling directions causes destructive interference at zero applied field and the whole pattern changes. The critical current modulates according to

$$I_c(\Phi) = J_0 A \left| \frac{sin^2(\pi\Phi/2\Phi_0)}{(\pi\Phi/2\Phi_0)} \right|. \tag{3.22}$$

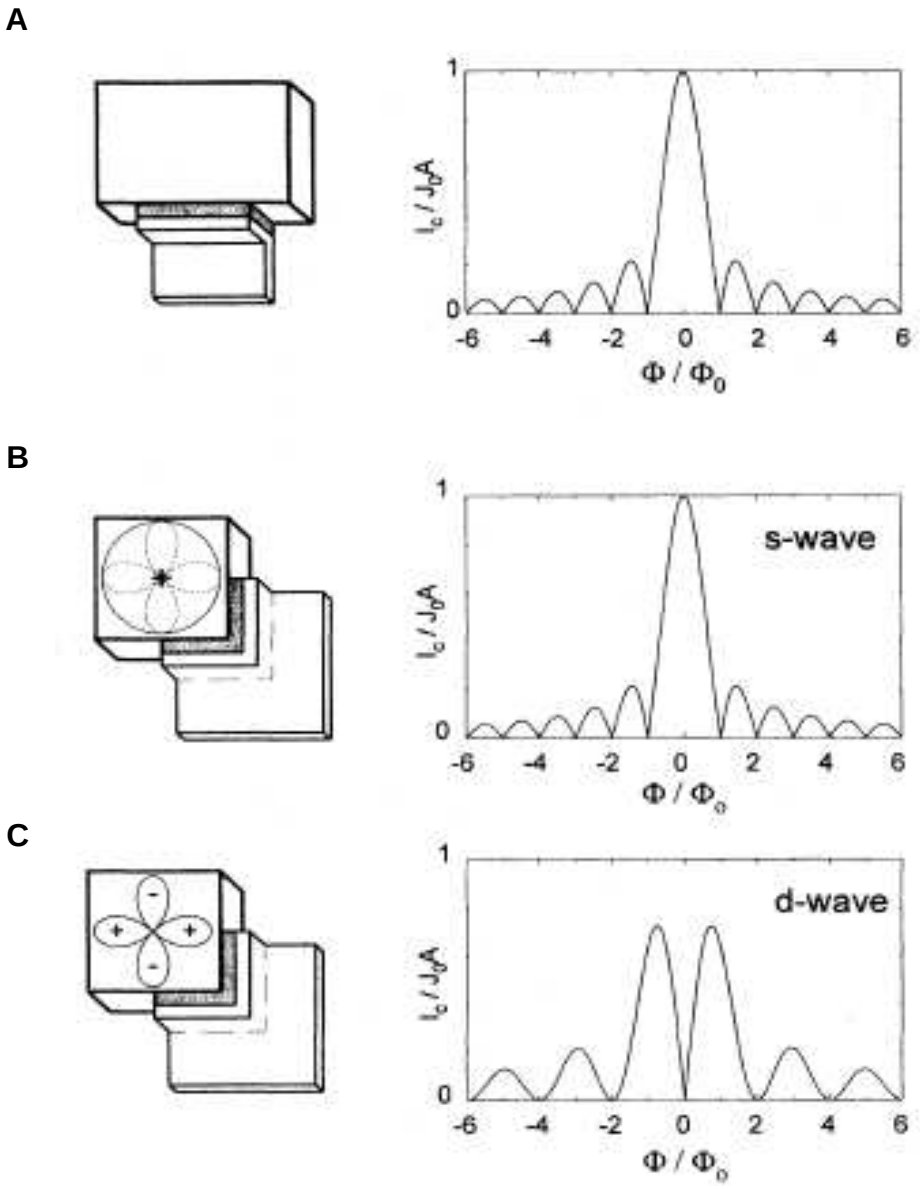

Figure 3.7 *Schematic of Josephson junctions with corresponding diffraction patterns. (A) Edge junction and (B) corner junction on a single crystal of s-wave symmetry both have a Fraunhöfer pattern while (C) a corner junction on a crystal of d-wave symmetry shows a different pattern. From [45].*

Such a pattern is represented in Fig.3.7(C). In a finite field, the critical current vanishes whenever there is $n\Phi_0$ flux quanta in each half of the junction, doubling the periodicity of the diffraction pattern. In this case, the distinguishing feature between the two possible order parameters is a maximum or a minimum at zero field.

There are a number of advantages to the corner junction experiment compared to the corner SQUID. First, the devices are easier to make. There is only one junction to fabricate, instead of two for the SQUID. They have a smaller area and hence have better odds of being on a more homogeneous area of the crystal. Second, asymmetry in the two sides of a single junction has much less impact than asymmetry in the SQUID: it only reduces the depth of modulation of the pattern. Third, the probability to trap vortices is lower since the device area is greatly reduced. Finally, the corner junction experiment could help identify a complex admixture of s- and d-wave order parameter in the material by the peaks becoming asymmetric and the dip moving away from zero.

The experimental results are presented in Fig.3.8. Although the modulations from corner junctions don't go to zero, probably because of junction asymmetry, the data shows a clear difference between diffraction patterns on edges and corner of YBCO single crystals and show strong evidence for a d-wave order parameter in the material. From the difference in peak heights, the authors put an upper bound of 5% on the possible s-wave admixture in the d-wave order parameter.

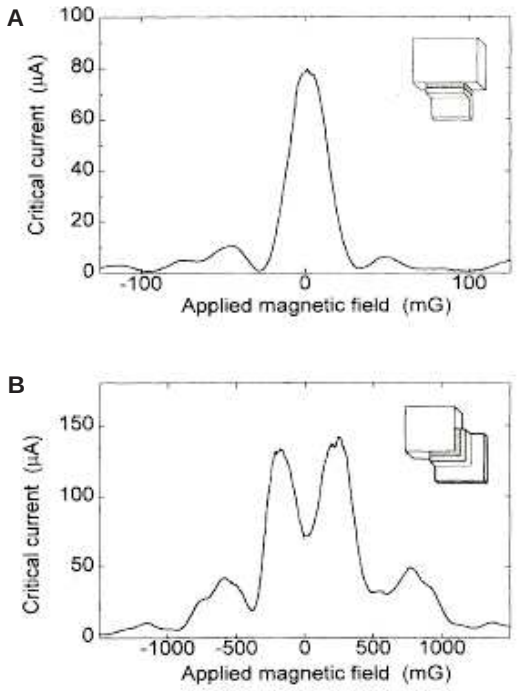

Figure 3.8 *Diffraction patterns measured on bimetallic YBCO-Pb devices with different geometries: (A)an edge Josephson junction, (B) a corner Josephson junction. From [48].*

3.3.3 Josephson interferometry in grain boundary junctions in cuprates

A grain boundary separating two different crystal orientations in cuprate superconductors causes, for a large enough misorientation angle, a Josephson junction to form at the interface. These are commonly called "grain boundary junctions" and have been thoroughly studied [49]. Some of these, the so-called 45 degrees asymmetric junctions where a given crystal axis in one of the grains is aligned with boundary and in the other grain the same axis is 45 degrees misaligned with the boundary, are of particular importance in trying to identify the complex component to the $d_{x^2-y^2}$ order parameter. Their geometry is illustrated in Fig.3.9.

In cuprates superconductors, the d-wave order parameter can be sup-

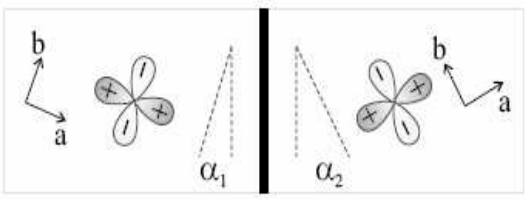

Figure 3.9 *Geometry of grain boundary junctions defined by the angles α_1 and α_2. Symmetric junctions have $\alpha_1 = -\alpha_2$ and asymmetric ones have $\alpha_1 = 0$. From [50].*

pressed at surfaces. In the 110 direction, Andreev reflection at the surface can create zero energy bound states that could suppress the d-wave order parameter and favor the formation of a subdominant complex order parameter that would break time reversal symmetry through an additional transition at a temperature T^*. Such an order parameter would have a significant effect on the diffraction patterns of Josephson junctions. In 45 degrees asymmetric junctions, the lobe and node of the d-wave order parameter face the interface on either side. That configuration should give a zero critical current if it wasn't for the facets at the interface: they allow tunneling from in-phase lobes or out-of-phase lobes, depending on the facet's orientation, as illustrated in Fig.3.10(A). In an applied magnetic field, the critical current modulates following a complicated pattern that reflects the details of the faceting along the grain boundary and the order parameter symmetry at the interface (See Fig.3.10(B)). The 45 degrees asymmetric junctions are in that aspect very different from other grain-boundary junctions whose diffraction pattern are closer to the Fraunhöfer pattern mentioned earlier (see Fig.3.10(C)).

In an extensive study of such junctions made of $YBCO$, undoped and doped with Ca, Co, Ni, and Pr; and $Bi_2Sr_2CaCu_2O_8$ ($BSCCO$) [50], the temperature dependence of diffraction patterns was measured to identify any evidence of subdominant order parameter in the form of a dramatic increase of the critical current at zero field and strong asymmetries appearing below

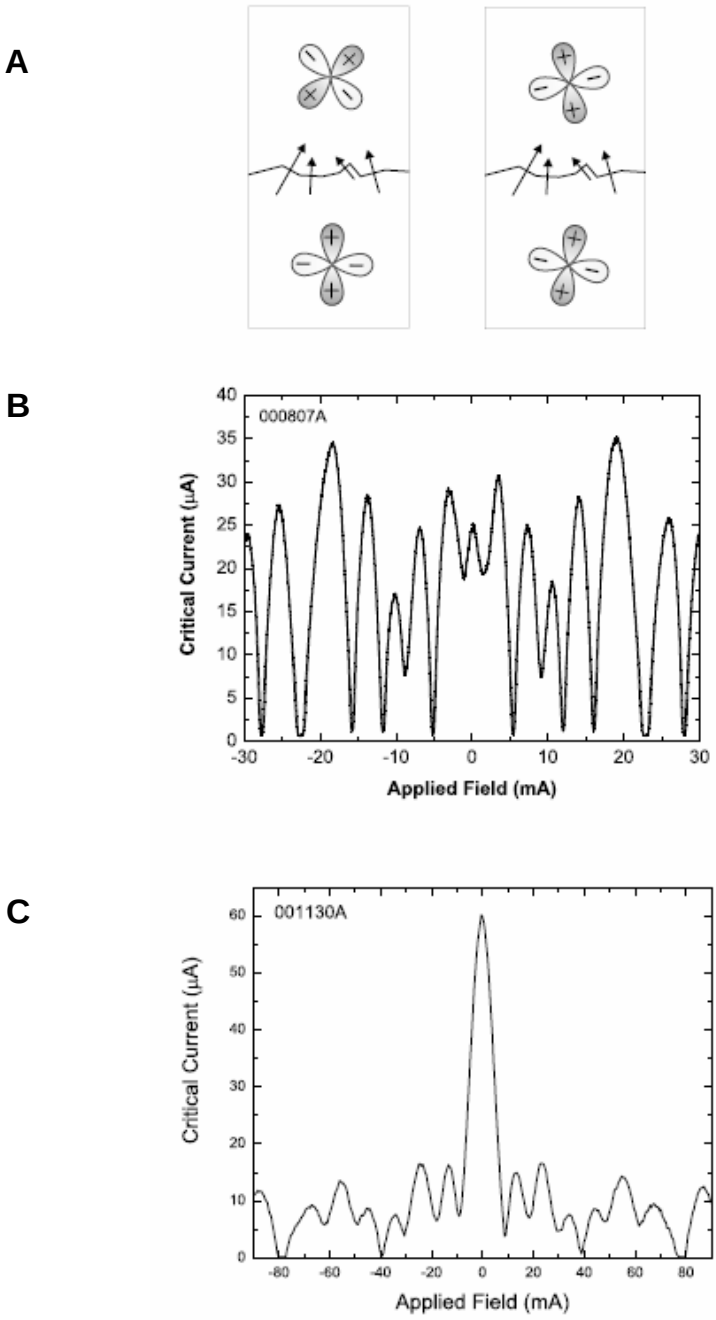

Figure 3.10 *(A) Asymmetric and symmetric 45 degrees grain boundary junctions with facetted interface. (B) The diffraction pattern of 45 degrees asymmetric grain boundary junction is very different from Fraunhöfer. (C) Fraunhöfer-like diffraction pattern of a* 45 *degrees symmetric grain boundary junction. From [50].*

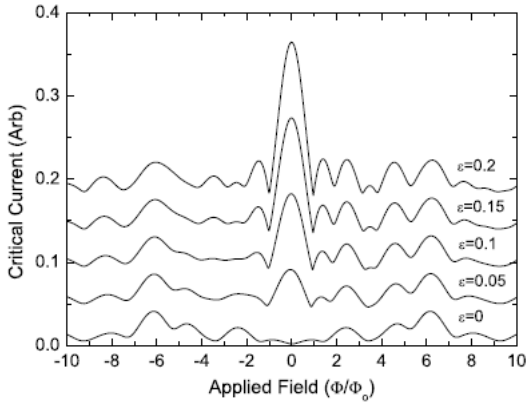

Figure 3.11 *Simulations of diffraction patterns for a complex order parameter $d + i\epsilon s$. As ϵ increases, the asymmetry in the pattern increases and a central peak appears, then increases. From [50].*

T^*. Computer simulations of the effect of an increasing complex component on the diffraction pattern are given in Fig.3.11. The increase in critical current happens because the order parameter with broken TRS is fully gapped, and hence below T^*, the scenario in Fig.3.9 changes to tunneling from a node to a lobe. The asymmetry in the diffraction pattern comes from intrinsic phase shifts across the facets of values other than 0 or π. They did not find evidence of the phenomenon in any of the compounds but reported evidence for second order Josephson tunneling in $BSCCO$ (See Fig.3.12). It is manifested by a central peak with a period that is half of that of the others and that has a different temperature dependence.

These experiments added a useful tool to the Josephson interferometry technique: they provided a diagnostic test for self-field effects in the junctions. As mentioned earlier, if the junction is larger than the Josephson penetration depth, the current at zero field is not uniform through the junction and it creates fields that distort diffraction patterns and can introduce asymmetries. In straight edge and corner junctions, the problem is avoided by making the junctions smaller than λ_J. In grain boundary junctions how-

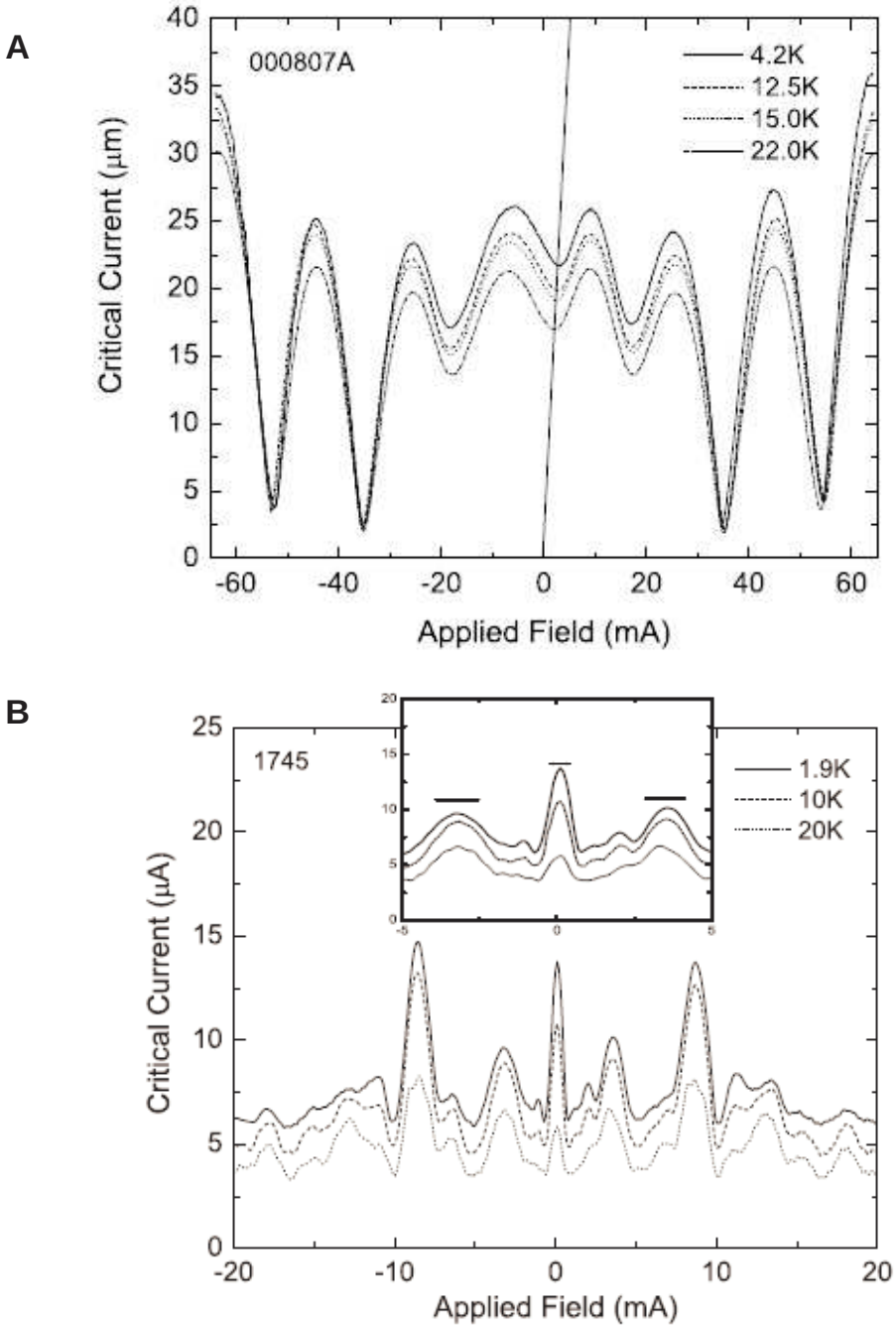

Figure 3.12 *Diffraction patterns measured on grain boundary junctions. (A)YBCO: the asymmetry with positive and negative field is due to self field effects. (B) BSCCO: evidence for a* $\sin 2\varphi$ *component in the Josephson current: the central peak is half the width of the others and has a different temperature dependence. From [50].*

ever, λ_J is not clearly defined. The measured critical current is an average of the critical currents of all facets. The actual λ_J that will dictate field penetration in the junction is a local quantity that varies from facet to facet whose corresponding critical current and junction size cannot be measured. One large low-angle facet will have a much larger current density than the others and will introduce self-fields effects in the junction even if a large number of small facets with current flowing in the opposite direction keep the measured critical current low.

Because they could not be avoided in junctions with grain boundaries, self-fields effects had to be accounted for. The method used is based on the fact that self-field effects do not break time reversal symmetry. Reversing both the direction of the applied current and the applied field is equivalent to reversing the direction of time. Hence, if diffraction patterns are measured for both positive and negative current directions and plotted on the same graph, features caused by self field are symmetric through the origin, while features caused by broken time reversal symmetry are symmetric with respect to the x-axis. An example of self field effects in a $10\mu m$ and 20% Pr doped YBCO junction is given on Fig.3.13.

3.4 Josephson coupling between singlet and triplet superconductors

3.4.1 Theoretical predictions

The Josephson effect between singlet and triplet superconductors has been a long standing issue. After the discovery of superconductivity in alloys containing ferromagnetic elements and the proposal of spin-triplet pairing in

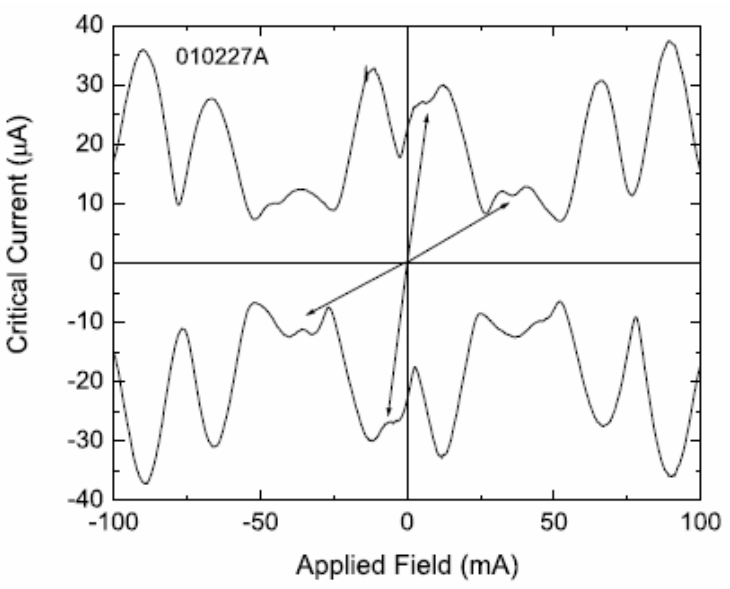

Figure 3.13 *The positive and negative of diffraction patterns with self-field effects are symmetric through the origin. From [50].*

those compounds, Pals *et al.* [51] calculated the Josephson coupling between singlet and triplet superconductors. They studied states conserving time reversal symmetry and without spin-orbit coupling and demonstrated that the Josephson currents are zero to second order in the tunneling matrix elements independent of the specific triplet state. That can be understood since there are no singlet spin states on the triplet side of the barrier for the singlet pairs to tunnel into and vice-versa. On symmetry grounds, the tunneling is forbidden because singlet and triplet states transform differently under time reversal (one is even and the other odd). Later, Fenton [52] showed that in the presence of spin-orbit scattering and spatial variations of the order parameter at the interface, there is a large amount of mixing between even and odd parity states that causes proximity and Josephson effects to be possible between the two. In the presence of spin-orbit scattering, the quasiparticles are not eigenstates of the spin and when they pass through the interface they have to transform from one spinor-state to another. Because of the difference

in spin-orbit scattering on the two sides of the junction, the Hamiltonian provides a spin-flip mechanism. He also pointed out that for junctions between conventional superconductors and heavy fermions, the critical current would be orders of magnitude smaller than in the singlet-singlet tunneling case because of the large difference in effective masses. Geshkeinbein and Larkin [53] also worked on the problem and took the crystal symmetry into consideration. They predicted larger critical currents for cases where the tunneling Hamiltonian becomes non-diagonal and a strong dependence of the coupling on tunneling directions. It is now agreed upon that in the presence of any spin flip mechanisms, first order Josephson tunneling does occur in singlet/triplet junctions.

Calculations have been done specifically for s-wave / Sr_2RuO_4 junctions [54] which we will be concerned with in the remainder of this work. Asano *et al.* assumed a chiral p-wave order parameter in Sr_2RuO_4 and introduced spin-orbit coupling as an interface effect. They found that besides spin-orbit coupling, a broken parity at the interface is necessary for finite Josephson current in the junction — the orbital parts of different parity are orthogonal unless the symmetry is broken. For a junction interface in the yz plane, they found that the spin-orbit coupling is associated with the component of the order parameter parallel to the interface and the current-phase relation of the junction is therefore also connected to the same component. For a pure p_x order parameter ($\hat{x} \perp$ to the interface), they found zero energy states at the interface and an associated low temperature anomaly in the Josephson current.

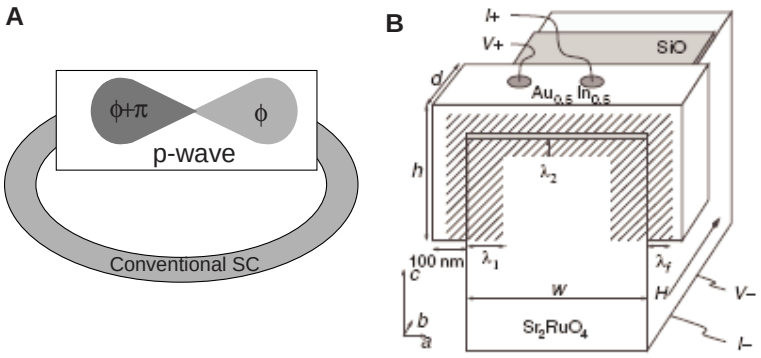

Figure 3.14 *(A) Schematic of a Geshkeinbein-Larkin-Barone Josephson device. (B) Realization of the device with Sr_2RuO_4 and $Au_{0.5}In_{0.5}$ from [28].*

3.4.2 Josephson interferometry of $Sr_2RuO_4/AuIn$ SQUIDs

The concept behind the experiment, using SQUID interferometry to detect odd orbital pairing in a superconductor, was first suggested by Geshkeinbein, Larkin and Barone [55]. They proposed a bimetallic device where a single crystal of an unconventional superconductor is used to close a loop made of a conventional one as shown in Fig.3.14(A).

If the unconventional superconductor is of odd pairing symmetry, there should be a phase difference of π from opposite faces of the crystal and the interference pattern should have a minimum at zero applied field. As pointed out by Asano *et al.* [56], a major concern in this experiment is that there is an arbitrariness of sign in the expression for the Josephson coupling. The lowest order matrix element is

$$\langle \psi_s(\mathbf{k})(\mathbf{k} \times \mathbf{n} \cdot \mathbf{d}(\mathbf{k})) \rangle_{FS} \tag{3.23}$$

where the average is over the Fermi surface, ψ and $\mathbf{d}$ are the singlet and triplet order parameters and $\mathbf{n}$ is the normal to the interface. The arbitrariness comes from the orientation of $\mathbf{n}$ that depends on the interface potential.

Depending on the details of how the parity is broken at the interface the experiment could be inconclusive. They made the assumption that all interfaces treat parity in the same way and their calculation show that indeed a critical current minimum at zero field, even in the presence of order parameter domains, would indicate odd pairing symmetry. Notice that even if the interface did not consistently treat the parity in the same way there would be a finite probability of the experiment yielding a maximum at zero field in the interference pattern and a finite probability of a minimum at zero result. The first would not give any information on the pairing symmetry of the system while the second would give proof of odd symmetry pairing.

The experimental results [28] for the test and the control devices are shown in Fig.3.15(B) which includes a schematic of the device they used. They had to address the same issues of loop inductance and current asymmetry mentioned for the corner SQUID experiments in cuprates. The fact that the maximum of the modulation shifts towards $\Phi_0/2$ in the test sample while it shifts towards zero in the control sample indicates odd symmetry pairing in the unconventional superconductor.

3.5 Effects of current inhomogeneities, facetting and trapped magnetic flux on the diffraction pattern of an edge junction

In an ideal case, diffraction patterns of edge junctions, i.e., junctions made on a straight edge of a crystal, should always give Fraunhöfer diffraction patterns. However, there are distortions of the pattern that come from a

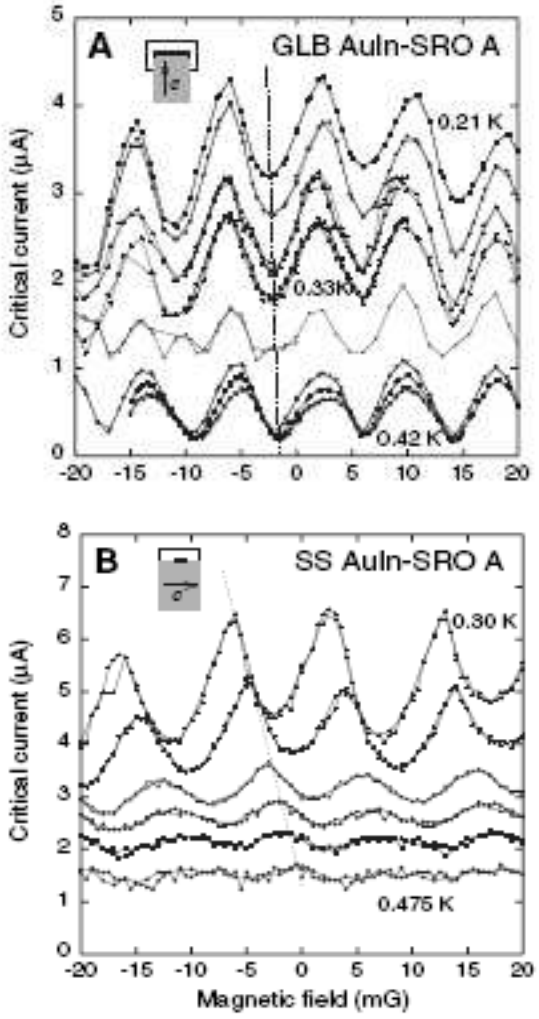

Figure 3.15 *SQUID interference pattern in Sr_2RuO_4/AuIn devices. (A) For junctions on opposite side the minimum extrapolates to zero field as the critical current goes to zero. (B) For SQUID with same side junctions, the maximum extrapolates to zero field. From [28].*

number of factors that tend to be present in experimental data. Here we present some simulations of their impact on the diffraction pattern in an effort to differentiate them from the intrinsic phase shifts.

3.5.1 Junction Simulations

We calculate diffraction patterns by integrating the critical current density given in Eq. 3.17 and maximizing the expression to find the phase φ_0 at the center of the junction which gives the maximum current for different values of applied field. The total current through the junction is given by

$$I = \int_{-w/2}^{w/2} J_c(y) \sin\left(\frac{2\pi\Phi(y)}{\Phi_0} + \varphi_0\right) dy. \tag{3.24}$$

In the most simple case, the critical current density J_c is a constant over the junction and $\Phi(y) = \Phi y$, in which case the integral, after maximization, gives a $(\sin x)/x$ Frauhöfer pattern. To incorporate current inhomogeneities, J_c becomes a function of y. Facets are added in the same way, except that they change both the magnitude of the critical current and the tunneling direction. For the simulations, the junction is divided into domains of random sizes with different J_c and random angles. In order to add in vortices, $\Phi(y)$ is not a linear function of y anymore. Instead, spikes in the field are added at positions where the vortices are introduced, the height and width of the spike reflecting the distance from the junction to the vortex.

3.5.2 Inhomogeneities in the current density

These originate from a tunneling barrier that changes across the junction either from rough interfaces between materials or an inhomogeneous tunneling layer. Even without simulations, one can see that they lead to distortions in

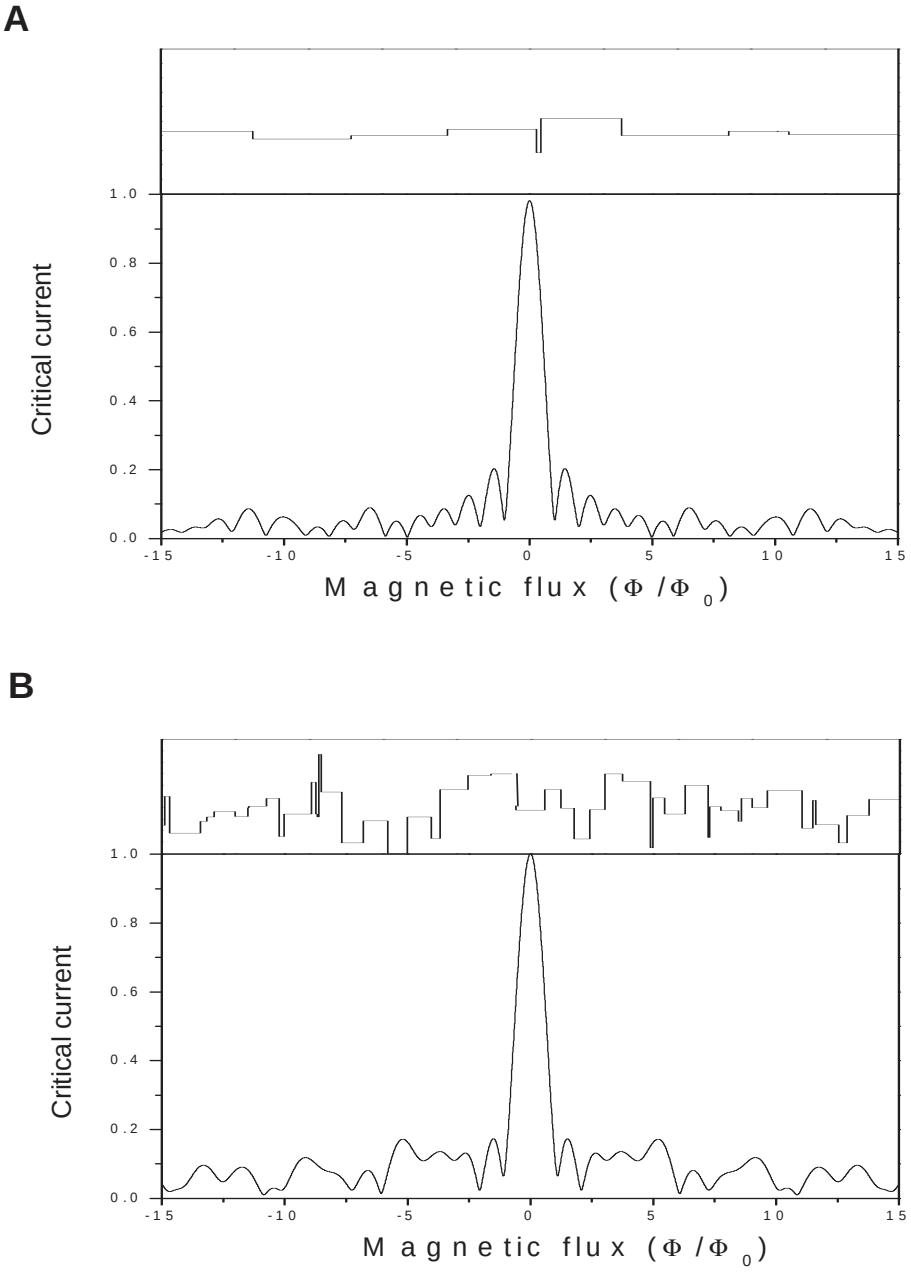

Figure 3.16 *Simulations of diffraction patterns for two inhomogeneous interfaces: (A) 10 regions of different critical current with a standard deviation of 0.2; (B) 50 regions of different critical current with standard deviation 0.5. The boxes above the patterns show the interfaces on the same scale.*

diffraction patterns, since for the extreme case of a hole separating two halves of the junction the pattern goes from a single junction diffraction pattern to a SQUID interference pattern.

Simulations of two cases with different levels of inhomogeneity are shown in Fig.3.16. As can be seen, the patterns are distorted but remain symmetric for positive and negative fields and they retain the central tall peak of the Fraunhöfer pattern. As can be expected, the more inhomogeneous the junction, the more distorted the pattern.

3.5.3 Facets in the junctions

In devices made of single crystals, the facets can be present if the crystal doesn't cleave properly and has a rough edge. As we mentioned before, facets introduce tunneling at an angle different from the normal to the interface. In an unconventional superconductor, the phase is anisotropic in k-space. Hence, the multi-directional tunneling introduces variable phase differences across the junction that can distort the diffraction pattern considerably. That's what happens in grain boundary junctions. Here we run simulations of facetted edge junctions between a conventional superconductor and a chiral p-wave superconductor and analyze the distortions introduced in the pattern for two different geometries as can be seen in Fig.3.17.

The amount of distortion depends on the phase difference that can arise between neighboring facets. It is worse for a d-wave order parameter because even small angle facets can pick up phase differences of π, the largest that can be sustained. That is the case for 45 degree asymmetric grain boundary junctions. The chiral p-wave order parameter shows much less distortion because the phase changes continuously and the phase differences between facets are proportional to the angle of the facet. An interesting feature of

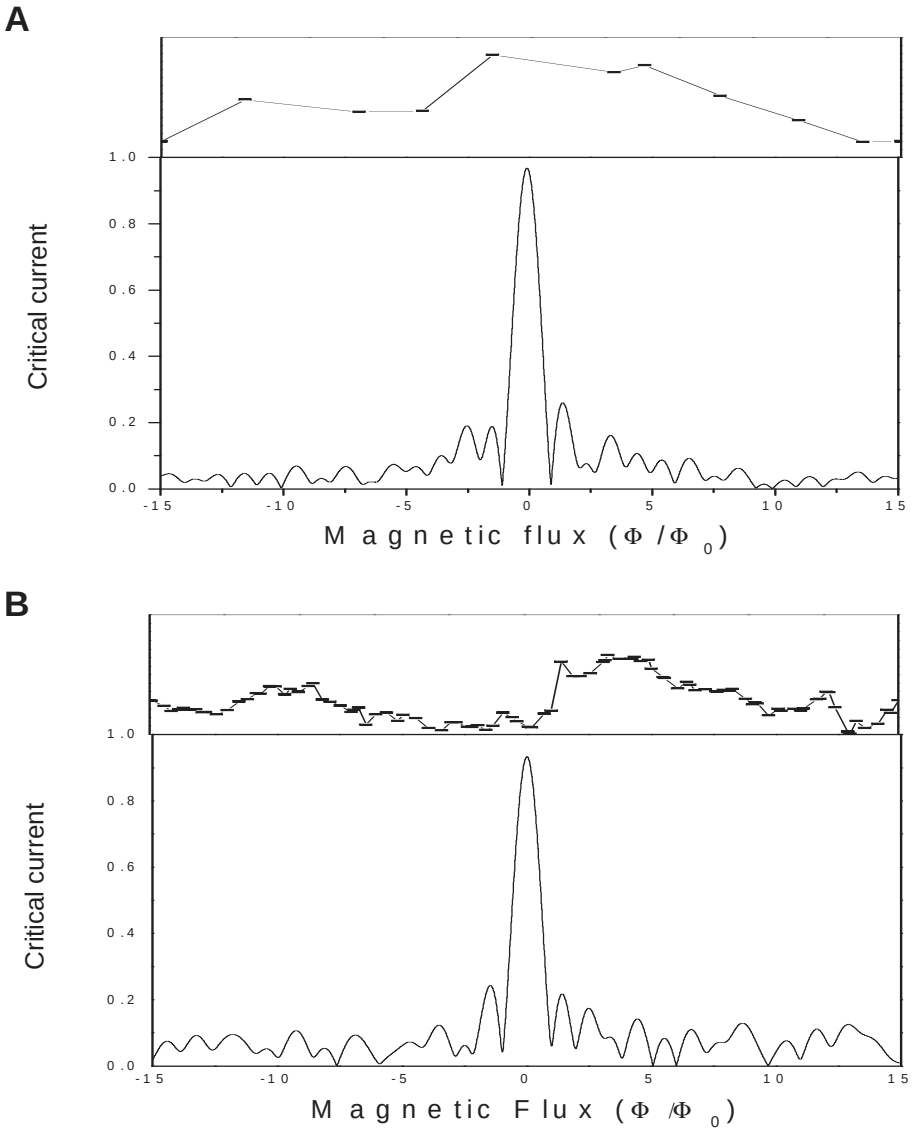

Figure 3.17 *Simulations of diffractions patterns for junctions between s and p-wave order parameter. (A) Junction with 10 facets at random angle; (B) junction with 100 facets at random angle.*

the distortions in junctions with p-wave order parameter is the asymmetry with field that appears in the patterns, evidence of the broken TRS.

3.5.4 Trapped magnetic flux

At the superconducting transition, any residual field in the experimental environment will either be screened out of the superconductor or become trapped in the form of vortices. The vortex has two effects on the diffraction pattern of the junction. First, it changes the effective field threading the junction. The spatially dependent field from the vortex gets added to the externally applied uniform field. Second, if the currents screening the field from the vortex flow across the junction, they contribute to the Josephson current and lower the critical current of the junction. When correctly positioned, vortices can mimic very convincingly an intrinsic phase difference in the material. Some examples of diffraction patterns distorted by vortices are shown in Fig.3.18.

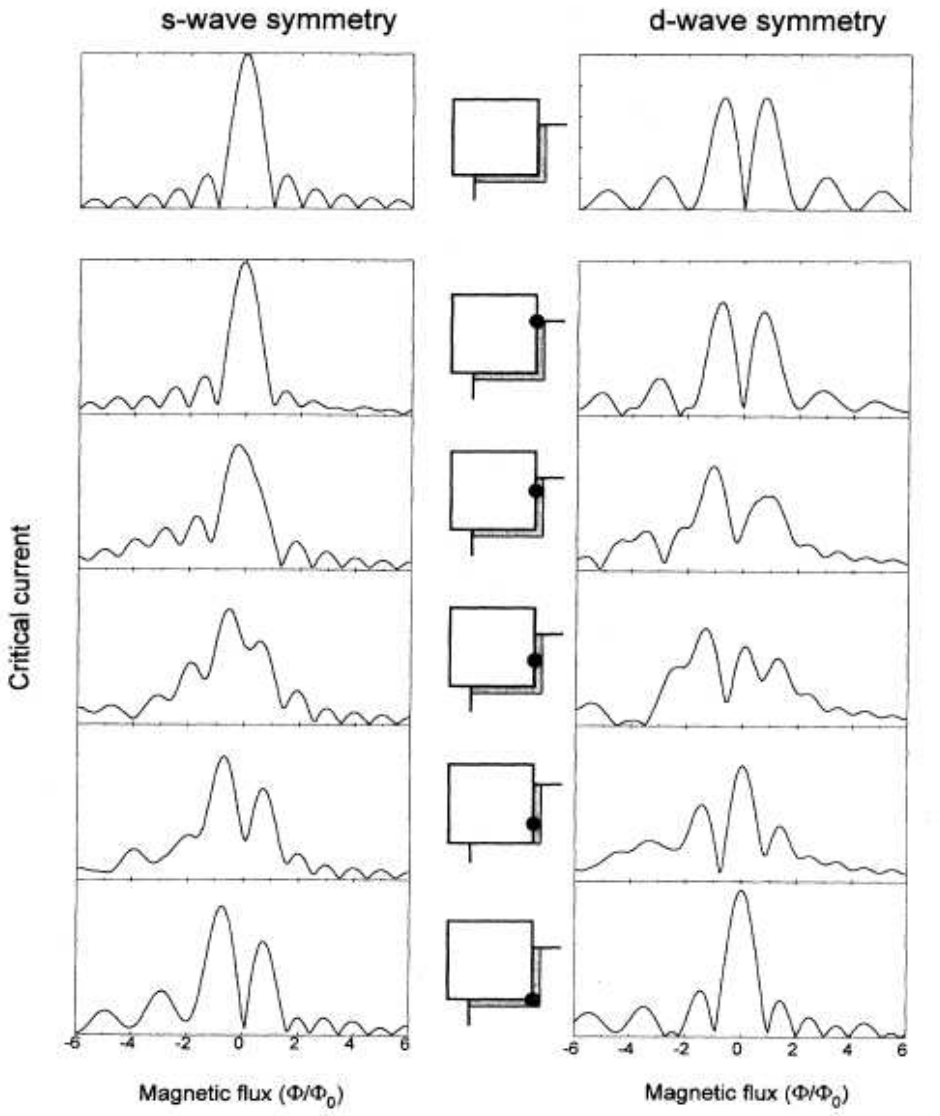

Figure 3.18 *Simulation of vortices in s and d-wave corner junctions. The vortices are at different locations as shown by the black dot. From [45].*

4 Technical experimental details

4.1 Crystal growth

The very high purity single crystals of Sr_2RuO_4 that we used for experiments were grown at Kyoto University in Prof. Yoshiteru Maeno's group. They are grown by a floating zone method in image furnaces where melting is achieved without the need for a crucible by focussing a light on the sample [57]. In this method, the bottom end of a feed rod suspended from above is melted and connected to a seed rod held from below. A single crystal is continuously grown from the molten solution by lowering both the feed and seed rods. The ceramic feed rod is made by solid state reaction between $SrCO_3$ and RuO_2, where particular attention is made to avoid Ba and Na impurities because they have been proven to degrade the superconductivity in the material [3]. The seed material can be either sintered polycrystals or a single crystal. Using the technique, the authors managed to grow large sizes of very high quality crystals with residual resistivity lower than $0.1\mu\Omega - cm$ and T_c as high as $1.49K$. A picture of the long single crystal rod that can be obtained is given in Fig.4.1.

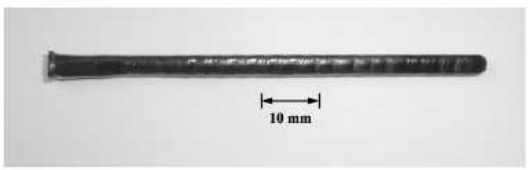

Figure 4.1 *Picture of a long rod of Sr_2RuO_4 single crystal. From [3].*

They found that the quality of the crystals, i.e., very low levels of impurity and defects associated with (1) high superconducting transition temperatures, (2) narrow transition width and (3) low residual resistivity, depend on the growth conditions. They also found that some growth conditions favor additional phases appearing through eutetic solidification: (1) Ru metal lamellae get imbedded in the main Sr_2RuO_4 when $2N(Ru)/N(Sr) \geq 1.2$; (2) epitaxial-like intergrowth of $SrRuO_3$ on Sr_2RuO_4 when ΔV is small and the oxygen pressure $P(O_2) \simeq 0.3$ bar (here, ΔV is the difference between the speeds of the feed and seed rods), (3) eutetic growth of Sr_2RuO_4 and a new insulating compound of unknown composition, possibly $Sr_3RuO_{5+\delta}$. The crystals used in the present study were tested by X-rays and magnetic susceptibility measurements to be free of any of these phases.

4.2 Junction fabrication

In order to make the Josephson junctions, a flat side of the crystal perpendicular to the ab-plane has to be exposed. We used two different methods for surface preparation. First we tried cleaving. It is in general the best type of surface preparation since it yields a very flat surface along the crystal axes. In the case of Sr_2RuO_4, it is not so easy to implement since the crystals are easier to cleave along the ab-plane than perpendicular to it. We found that once they were cleaved to be very thin, with a height of less than $500\mu m$, they also cleave in the direction parallel to the c-axis but with a small yield: about 1 out of 10 samples are smooth enough to make junctions.

Polishing is an alternative way of surface preparation. It is more reliable, allows for larger surfaces and the possibility to use multiple sides of the crystal. We mounted the crystals on a microscope cover slide using the epoxy

crystal bond and polished it with different grits of sandpaper, finishing with diamond lapping films for a finish as smooth as $0.1\mu m$. Because polishing damages the sample, we weren't able to make Josephson junctions on polished sides without an annealing step after the polishing at 1000 degrees Celsius in air for 24h. Even after annealing, the critical current density of polished samples remained orders of magnitudes lower than that of cleaved samples. They also have a much lower junction resistance. This comes as a surprise, since a low resistance barrier is usually associated with high critical current.

After preparing the surface, the junctions were made following a recipe established by David Wollman, a former group member [58]. The crystal is glued on a glass substrate using polyimide, a chemical sometimes used as photoresist. It was chosen for its good thermal expansion/contraction properties over a large temperature range and the fact that it goes slowly through different viscosity stages when drying, which is very useful in controlling the height of the junction. Another advantage is that, after being properly cured, it is compatible with a high vacuum. The polyimide has to come up the side of the crystal in order to provide a smooth bridge for the metallic film going from the substrate to the side of the crystal. The crystal is then masked using a roll on resist as a flexible mask. A picture of the masked crystal is given in Fig.4.2.

Next, the crystal is loaded into a vacuum chamber where it is ion milled for cleaning purposes and a normal metal followed by a superconductor are thermally evaporated. The sample stage has to be rotated so that the superconductor can be evaporated on both the edge of the crystal and onto the substrate. A cartoon of the geometry in the deposition chamber is given on Fig.4.3. We found that there was no need for a substantial normal metal barrier since the crystals seem to have a normal metallic layer at the surface,

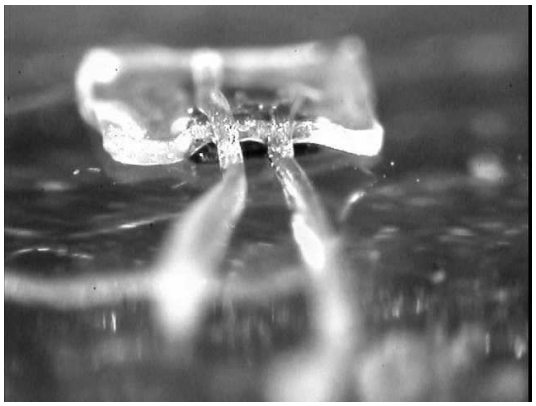

Figure 4.2 *Masked Sr_2RuO_4 single crystal.*

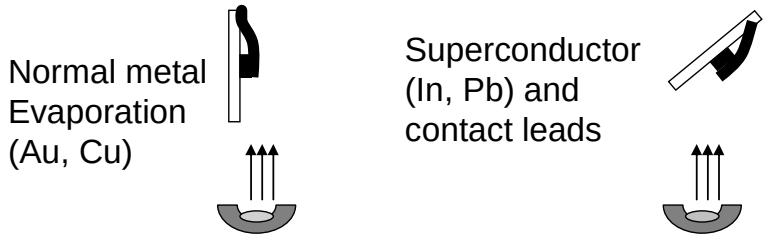

Figure 4.3 *Evaporation geometry for normal metal and superconductor during the junction fabrication.*

probably too disordered to be superconducting. Despite that, when no normal metal was deposited, the devices were resistive. It is not very clear why, but we speculate that the Pb or In diffuses into the crystal and suppresses the fragile superconductivity in a layer too thick to preserve a weak link. The final recipe we adopted consisted of using a very thin layer of normal metal (10 to 20 nm) that probably serves as a separation between the crystal and the other superconductor. The superconducting film has to be very thick ($\sim 800nm$) in order to remain continuous across the glass, the glue and the crystal at low temperatures.

We successfully made junctions with different metals: Au and Cu for normal metals, In, Pb, Al and $PbIn$ for conventional superconductors. Au did not wet the crystal very well and gave very inhomogeneous junctions. We used Cu and Pb in most of the junctions we measured. A picture of a

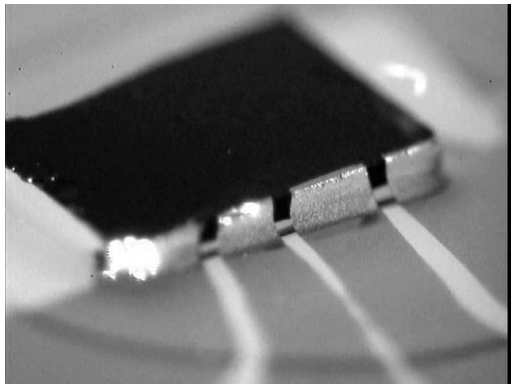

Figure 4.4 *Picture of a typical device. The black rectangle is a Sr_2RuO_4 single crystal and the gray stripes are the Pb film.*

typical sample is shown in Fig.4.4.

The junction sizes vary from $20\times50\mu m$ to $100\times300\mu m$. Because of the low critical current densities, the junctions should belong to the small junction limit as defined in the previous chapter, despite their large areas. If, as the data seems to indicate, they contain order parameter domains with currents flowing in opposite directions, the Josephson penetration depth cannot be defined using the net critical current. As explained in the case of grain boundary junctions, there is no foolproof way of knowing if the junctions are indeed in the small junction limit.

4.3 Measurement Setup

The measurements were done in two different cryogenic systems: a commercial ^{3}Helium refrigerator from Oxford instruments ($Heliox2^{VL}$) with a base temperature of $\sim 325mK$ and a regular ^4He cryostat where the temperature would only reach $\sim 1.3K$.

4.3.1 Setup in ^{3}Helium refrigerator

The ^3He refrigerator is in a vacuum can that sits in a ^4He bath. ^4He is drawn from the bath to the 1K pot, where it is pumped on to reach a temperature of ideally 1K, but more often higher ($\sim 1.5K$), hence the name. The ^3He is in a closed cycle with a dump at the top where the gas stays after evaporation, a pot at the bottom where it collects when liquefied, and a charcoal sorb that can absorb the ^3He when cooled and release it when heated. The sorb is cooled by drawing ^4He from the bath and has a heater attached to it. The ^3He space is thermally connected to the 1K pot, which allows the ^3He gas to liquefy after it condenses at 3.2K. The liquid ^3He, now as cold as the 1K pot, is then pumped on by the sorb to reach a temperature on the order of 300mK, that varies depending on the heat load. It operates in a "single shot" mode: once condensed, the ^3He continuously boils at a rate that depends on the experimental heat load until the ^3He pot is empty. The system warms up to $\sim 4K$ and the ^3He needs to be recondensed. For proper operation, the vacuum needs to be very good in the can so that the different components of the insert can steadily hold different temperatures without exchanging heat. That is achieved by having a second charcoal sorb anchored to the 1K pot that absorbs all the gas remaining in the vacuum can below 5K. In our experiments, the biggest heat loads gave a hold time at base of 1 to 2 hours and once filled, the dewar would hold helium for about 20h.

In the system, the sample is thermally anchored at the bottom of the ^{3}He pot with a thermometer and a heater attached on the same bloc. A Helmholtz coil provides a magnetic field along the c-axis of the crystal necessary for the measurements. For samples with a low critical current, cold resistors are added to the lines carrying the electrical signal for noise filtering. For samples

with high critical current, the resistors generate too much heat and have to be bypassed. Around the vacuum can in the ^{4}He bath, a *Pb* superconducting can is used as a shield against magnetic field fluctuations from the outside. Additional magnetic shielding is provided by a double layer of mu-metal, a high magnetic permeability alloy that reduces the ambient field by orders of magnitude.

4.3.2 Setup in ^{4}Helium cryostat

This is a very simple system where the insert gets cold by submersion into a bath. The ^{4}He bath is cooled to temperatures lower than 4.2K by pumping on it. With the pumping power we had, the system's base temperature was 1.3K. The sample is isolated from the bath by a vacuum can that has some exchange gas and a charcoal sorb inside. That allows us to heat the sample independently of the bath if necessary: the cooled sorb absorbs the exchange gas decoupling the sample from the bath and when it is time to cool the sample again, the sorb is heated, releases the exchange gas and allows the sample to cool. As in the previous setup, the sample stage has a thermometer, a heater and similar filtering and shielding. This insert has two different coils that can provide fields both along the *c*-axis and in the *ab*-plane of the crystal.

4.3.3 Transport measurements

The primary measurements done in this study are current-voltage characteristics (IV) and diffraction patterns. The current is applied using custom made low noise battery-operated current supplies. Depending on the junction resistance, the voltage is measured one of two ways: For junction resistances

larger than $1m\Omega$, it is measured using a low noise commercial pre-amplifier (ITHACO). For lower resistances, the pre-amplifier cannot not resolve the voltages and we had to implement a SQUID potentiometer circuit. A diagram of the circuit is given in Fig.4.5(A). This setup uses the capability of the SQUID to detect very low values of magnetic field through a change in the critical current. A standard resistor and a pick-up loop are in series and are mounted in parallel with the junction. The standard resistor is a known resistor that doesn't change much with temperature and for the best detection level should be comparable with the junction's normal state resistance. We used brass foil as standard resistance for these experiments, the size of the foil determining the resistance ($m\Omega$ range). The pick-up loop couples inductively the system to the SQUID: a current flowing through the loop generates a field that modulates the critical current of the SQUID. If the SQUID is biased at a constant current I_{bias} that slightly exceed the critical current as shown in Fig.4.5(B), the change in critical current from I_{c1} to I_{c2} translates as a change in the SQUID voltage from V_1 to V_2. When the applied current is smaller than the junction's critical current, all the current flows through the junction and no SQUID voltage is detected. As soon as the applied current exceeds the junction's critical current, the current divides between the two branches according to the respective values of the standard resistor R_{st} and the normal state resistance of the junction R_n. Current starts flowing through the pick-up loop and the SQUID detects a finite voltage. If R_n and R_{st} are comparable in size, the SQUID voltage mimics that of the junction and the shape of IV using the SQUID or junction voltage is the same. The actual voltage across the junction and an accurate measure of R_n have to be calculated from the raw data using the SQUID transfer function.

We measure diffraction patterns three different ways. The simplest method

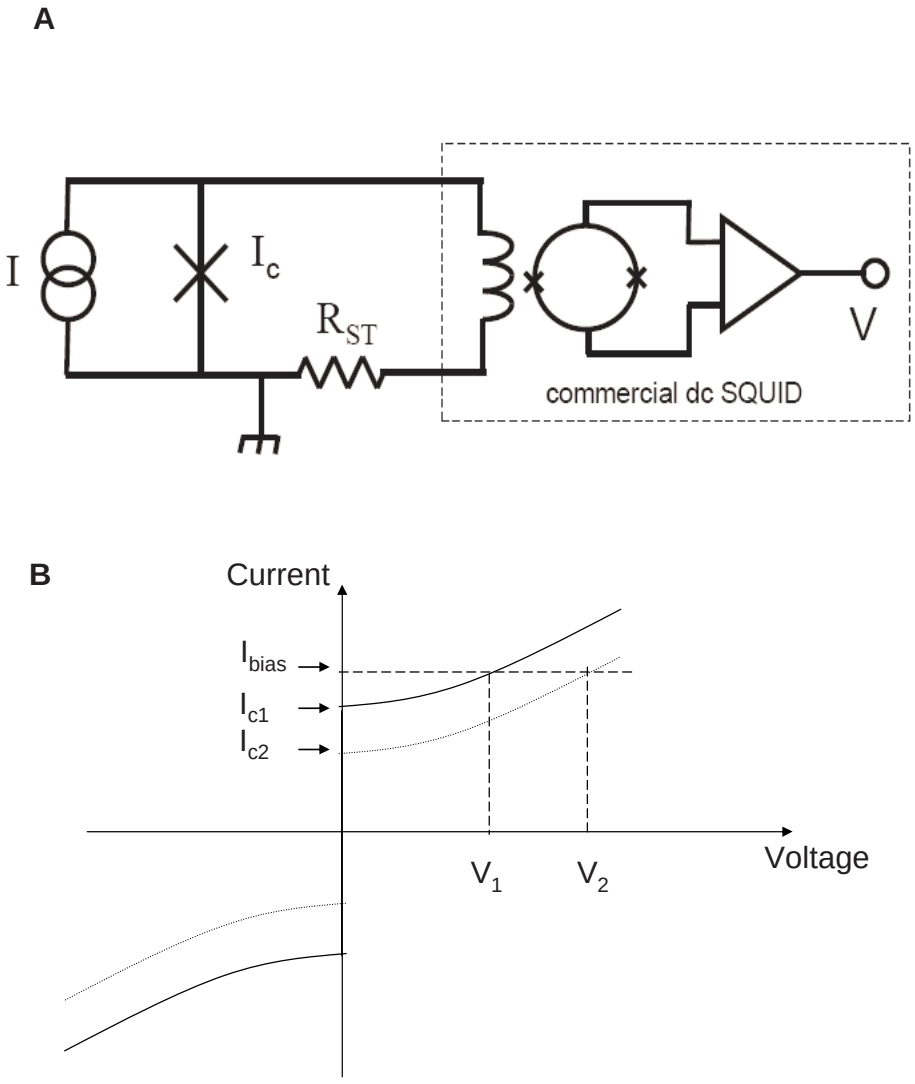

Figure 4.5 *(A) Circuit diagram of a SQUID potentiometer. (B) The voltage across a junction biased at a current exceeding slightly the critical current mimics the modulations of the critical current with the opposite sign: as I_{c1} decreases to I_{c2}, V_1 increases to V_2.*

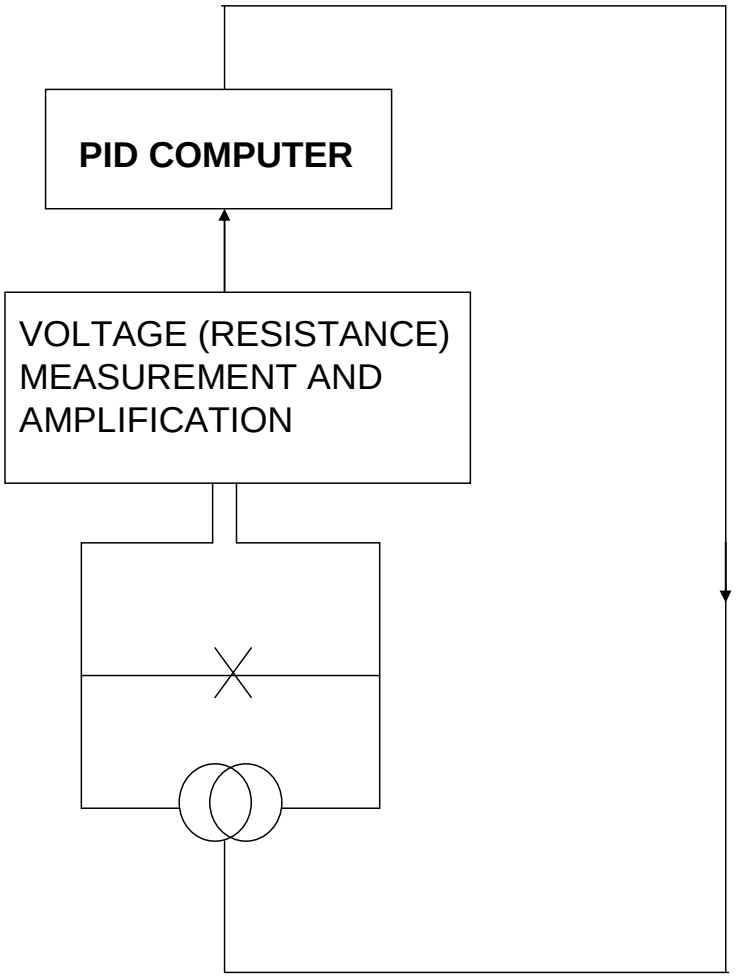

Figure 4.6 *Schematic of the experimental setup used to measure the critical current. A computer uses a PID program to maintain the current bias constant.*

(VPhi) measures the voltage modulations of a junction that is current biased slightly higher than the critical current as a function of applied field. As the junction critical current modulates, the voltage follows the modulations but with an opposite sign: a critical current increase translates into a voltage decrease and vice-versa, just like for the SQUID, as shown in Fig.4.5(B).

The other two methods directly measure the critical current by using a feedback loop that keeps the junction's voltage or dynamic resistance constant. A schematic of the experimental setup is given in Fig.4.6. Two com-

puter programs are used simultaneously: one controls the field and acquires the data, i.e., the current output to the junction and to the coil, and the other one measures the voltage (resistance) and adjusts the current output to the junction to maintain the voltage (resistance) to a set value using a PID program. The PID program is a widely used control loop that uses the Proportional, Integral and Derivative of the difference between a time-varying process variable and the set point to maintain a physical quantity to the set value.

Each of the 3 methods has its advantages and disadvantages which will determine when they are used. The first method, VPhi, is very easy to implement and is a direct measurement of a property of the system. Because of that, it is used for quick diagnostics and in cases where a high level of noise or very sharp data features could make the PID program significantly lag or lose track of the set parameter. Its disadvantages are that, first, it doesn't give the value of the critical current for all field values and, second, as the critical current gets farther from the current bias point, the accuracy of the data is greatly reduced. The second method, PID control with voltage criteria, solves the problems associated with the VPhi method and allows for a precise measurement of the critical current for all field values. When using it, one has to carefully monitor the set point and process variable and make sure that they remain in good agreement. Another problem that can occur is that if the instrument measuring the voltage drifts, then the apparently constant set point really corresponds to a varying position on the IV curve and the measurement is no longer accurate. It works best when using the SQUID for voltage measurement because of the increased precision. The third method, PID control with a resistance criteria is an improved version of the second one since it addresses the voltage drift problem. Even if the

voltage drifts, the resistance is a property of the junction and doesn't change. The cost is an increased complexity of the circuit. The resistance is measured using a lock-in technique that requires adding a small ac signal to the dc bias current and detecting the in-plane voltage response.

5 Evidence of order parameter domains and domain dynamics

The data presented here was taken on a large number of edge Josephson junctions. Their sizes and critical currents vary over orders of magnitude but they behave overall in a similar, although not identical, manner. Some exhibited features that others lacked. For each observation, we show the data that best emphasizes the point we are trying to make, although that behavior might be more modest or not present in other samples. We only present properties reproduced in many samples. All the junctions used in the study, together with their properties, are listed in a table in appendix A. The results in this chapter have been reported in [59].

5.1 Junction characterization

The current-voltage characteristics (IV) of the junctions showed the resistively shunted junction behavior expected for an SNS Josephson junction. An example of an IV is shown in Fig.5.1. To ensure that the junctions are due to tunneling into Sr_2RuO_4 and are not weak links in the conventional superconductor, we measured the critical current and the dynamic resistance as a function of temperature. We found that in some of the junctions, the critical current vanished at $\sim 1.5K$ as expected while others exhibited a supercurrent to higher temperature, up to $3K$. We attributed those higher transition temperatures to the presence of trace amounts of the $3K$ phase of Sr_2RuO_4, a well documented superconducting phase in the material that

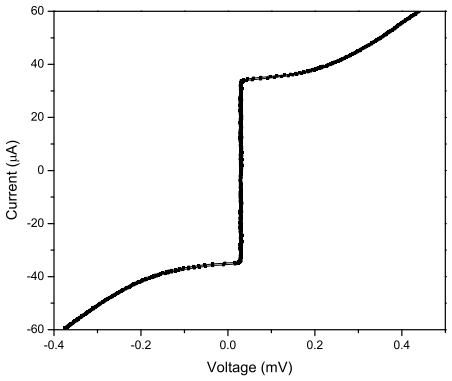

Figure 5.1 *IV characteristic of a $Sr_2RuO_4/Cu/Pb$ junction showing the expected resistively shunted junction behavior.*

occurs around Ruthenium inclusions [3]. An example of each case is shown in Fig.5.2. In the junctions with a higher T_c, the temperature dependence of the critical current changes slope at $1.5K$ (See Fig.5.2B), additional indication of the high temperature portion being caused by a different phase (it follows a different order parameter). We did not observe any different magnetic field behavior in the junctions with a higher T_c.

5.2 Qualitative differences in diffraction patterns

As we made more junctions, we noticed that their diffraction patterns were qualitatively different. Since these are edge junctions, we expected Fraunhöfer patterns for all of them. Some were close, with a central tall peak and side lobes, while others were completely different and were reminiscent of diffraction patterns for grain boundary junctions. A few of these patterns are shown for example in Fig.5.3. They are all asymmetric with field, which can only have three explanations: trapped flux, self field effects in the long junction

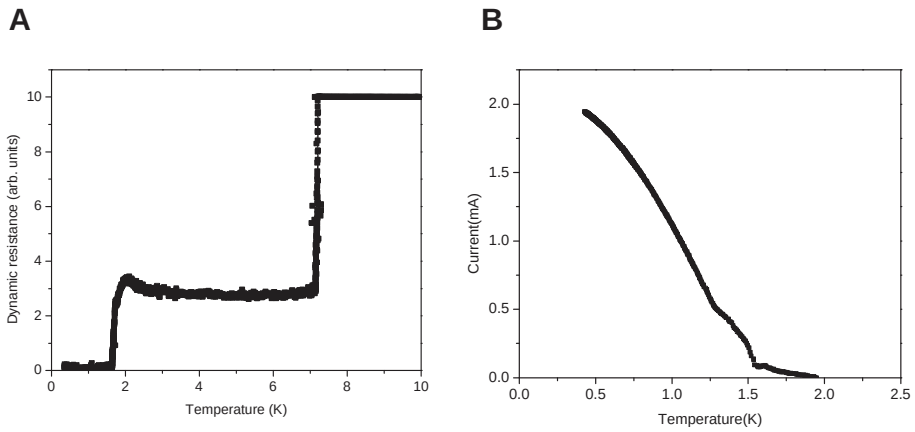

Figure 5.2 *Transition temperature of the Sr_2RuO_4 junctions measured by (A) Dynamic resistance: the drop in resistance at 7.3K shows the Pb transition while the drop at 1.5K shows the junction's transition; (B) Critical current: there is a tail in the critical current for $T > 1.5K$ with a different slope probably coming from trace amounts of the 3K phase.*

limit or a complex order parameter. The self-field effects are ruled out for the most part by measuring the junction at higher temperatures, closer to the T_c of Sr_2RuO_4. In that regime, the critical current is much lower and the junction falls in the short junction limit. Also, reversing the polarity of the applied current as explained in the previous chapter did not show symmetry through the origin. We first considered if the patterns in Fig.5.3 (B, C and D) could be explained by disorder (inhomogeneous barrier, facets, interface roughness). However, we observed that upon thermal cycling, the patterns changed as seen in Fig.5.3 (C and D). Since the junction's physical parameters are set by the fabrication, it is clear that the phase interference has to be a property of the superconducting state. The most likely candidates are either vortices or the presence of order parameter domains. As shown by the simulations in chapter three, adequately positioned vortices can distort the critical current modulation patterns significantly. Domains also provide a good explanation because they allow for regions of different phases to be side by side in a single junction which causes interference. If the phase dif-

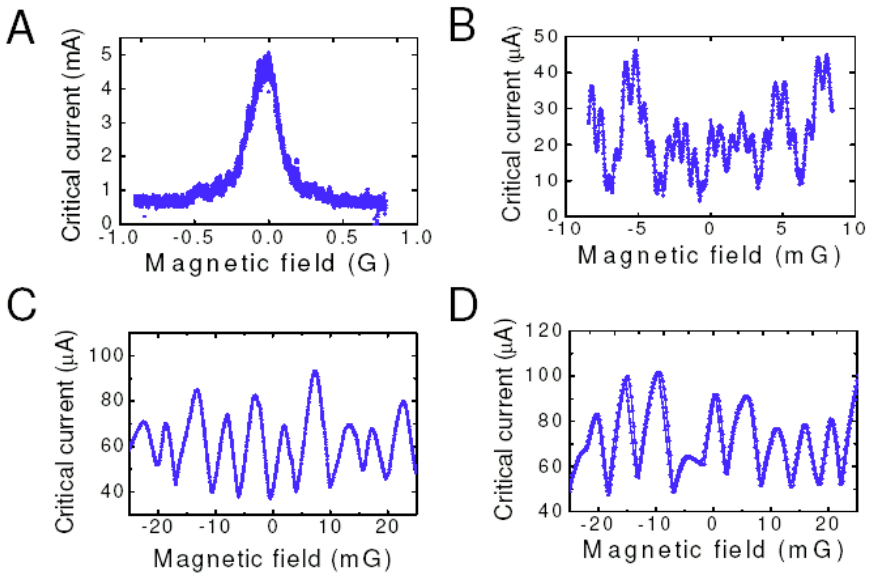

Figure 5.3 *Diffraction patterns of three different Sr_2RuO_4 junctions. (A) Fraunhöfer-like pattern, (B)and (C) Grain-boundary like patterns reflecting phase interference, (D) Pattern on the same junction as (C) after thermal cycling.*

ference is exactly π, we recover the case of grain boundary junctions, hence the similarity in the patterns.

Another surprise came as we measured junctions on orthogonal sides of the crystal. For two out of four samples measured with junctions on both sides, the diffraction patterns are qualitatively different on the two sides: one is Fraunhöfer-like with a large central peak while the other is similar to that obtained in grain-boundary junctions with a multipeak diffraction pattern. The two patterns are shown in Fig.5.4 (B and C). It could of course be a coincidence that domain-free regions happen to exist on one side of the crystal while domains form on the orthogonal side. However, a more plausible explanation is the presence of "parallel order parameter domains" as shown on the schematic in Fig.5.4 (A). A computer simulation of the diffraction pattern in that case is given in Fig.5.4(B and C). The domains are "chiral" domains, i.e., the phase changes its winding direction from clockwise

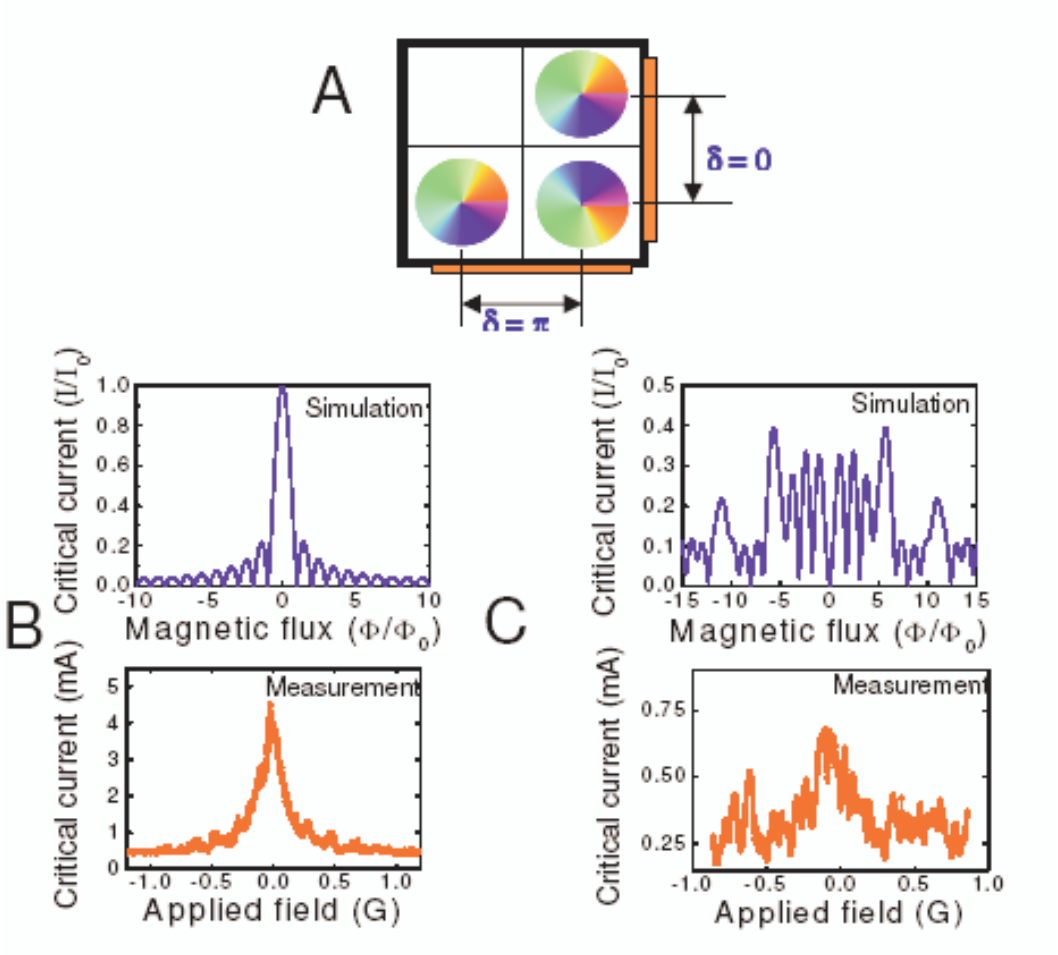

Figure 5.4 *(A) Graphical representation of a Sr_2RuO_4 crystal with parallel chiral domains showing the order parameter phase winding in opposite directions. The phase difference between domains, δ is zero in one tunneling direction and π on the orthogonal face. (B), (C) Measurements and computer simulations of the diffraction patterns for junctions on orthogonal crystal faces. (B) shows patterns corresponding to the $\delta = 0$ and (C) shows patterns corresponding to $\delta = \pi$. The simulations are done with 10 parallel domains of random size.*

to counterclockwise. We call these parallel domains because all the domains are in phase for a given tunneling direction, i.e., the real components align.

This brings up an important point. Because the phase is a relative quantity, its value at any point is arbitrary. However, once set at one point, all other connected points have a known phase. For this reason, although talking about a phase in a given direction in a superconductor usually wouldn't make sense, in the presence of domains the phases across domain walls are set by energy considerations and the phase inside a domain for various directions is set by the chirality of the order parameter such that the phase difference between two domains in a given direction in k-space is a well defined quantity. The phase difference between neighboring domains depends on the orientation of the order parameter in the domains and on the tunneling direction.

For parallel chiral domains, the phase is the same along the x-axis and the diffraction pattern of a junction made on the face normal to that tunneling direction is Fraunhöfer-like, while along the y-axis the phase difference is π and the diffraction pattern is similar to that of GB junctions.

The other two samples with junctions on orthogonal sides showed a different behavior, an example of which is shown in Fig.5.5. Here, the interference seems to be coming from phase differences that are not zero, nor π. We propose another domain geometry, "perpendicular domains", to explain our observation. Simulations for perpendicular domains are given in Fig.5.5. There is no tunneling direction where the domains are in phase.

We should note that for all samples with junctions on orthogonal sides, we systematically observe higher critical currents by at least one order of magnitude on one side compared to the other. It is not clear whether it is an intrinsic property of the junction or a consequence of the sample fabrication

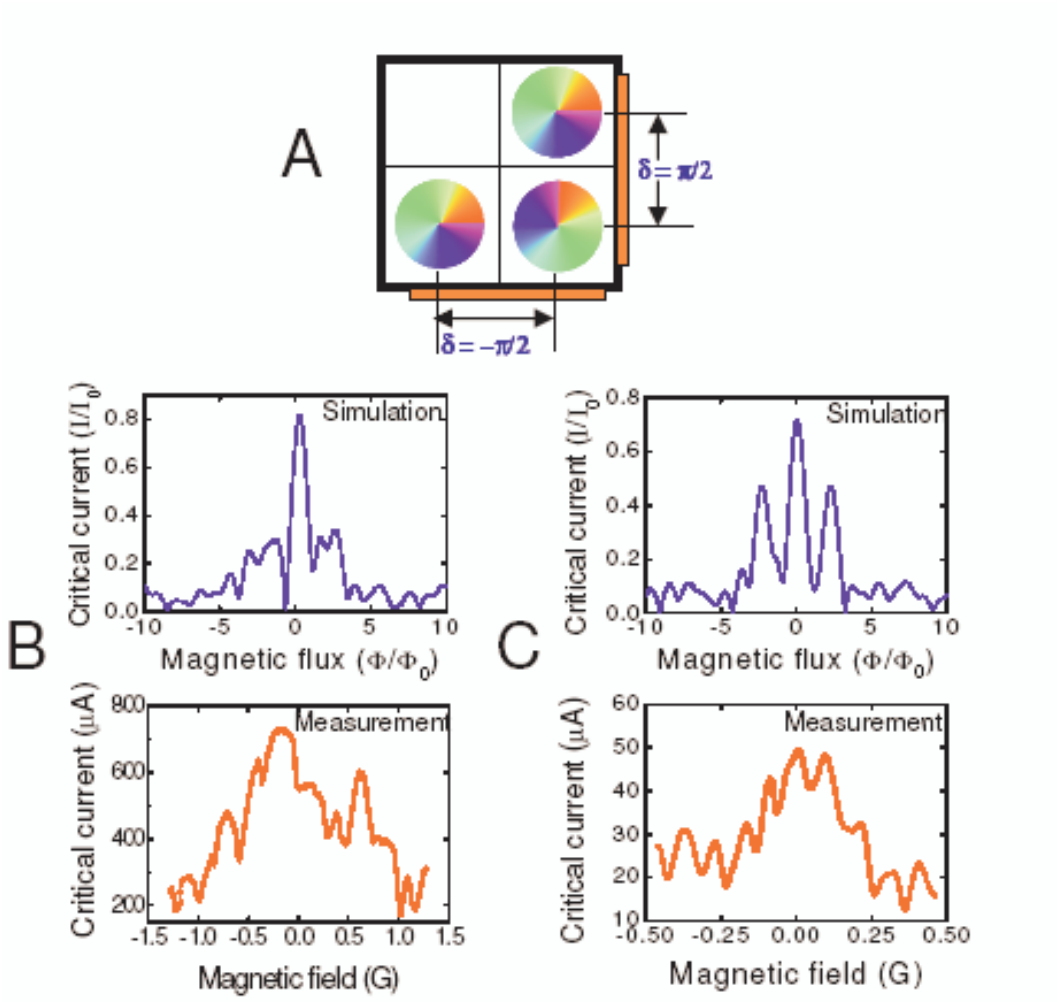

Figure 5.5 *(A) Graphical representation of a Sr_2RuO_4 crystal with perpendicular chiral domains showing the order parameter phase winding in opposite directions. The phase difference between domains, δ, is $\pi/2$ in one tunneling direction and $-\pi/2$ on the orthogonal face. (B), (C) Computer simulations of the diffraction patterns for junctions on orthogonal crystal faces with 10 domains of random size, compared to measurements on those junctions.*

process. The side that was last ion milled during fabrication could be cleaner and hence give better interfaces.

5.3 Domain dynamics: hysteresis and switches

5.3.1 Hysteresis

When a large enough magnetic field is applied, the diffraction patterns become hysteretic. The value of the threshold field is junction dependent. We observe two distinct types of hysteresis: in some of the junctions, once the threshold field is passed, the hysteresis continuously increases with field as shown in the first three patterns in Fig.5.6; in others, the hysteresis increases in discrete steps of field as in Fig.5.7.

In both cases, the hysteresis disappears when the maximum ramp value of the field is dropped below the hysteresis threshold, as shown in the two bottom traces in Fig.5.6. Sometimes the pattern looks different after a high field hysteretic sweep. In the example given in Fig.5.8, the pattern in (A) is the original pattern, (B) shows the high field sweep where the pattern does not retrace at all for the two sweep directions . The first low field sweep after the high field is applied (see Fig.5.8(C)) is hysteretic for the positive branch but retraces in the negative branch and the next pattern completely retraces but is totally different from the one given in (A). This behavior was observed in most of the junctions with hysteresis.

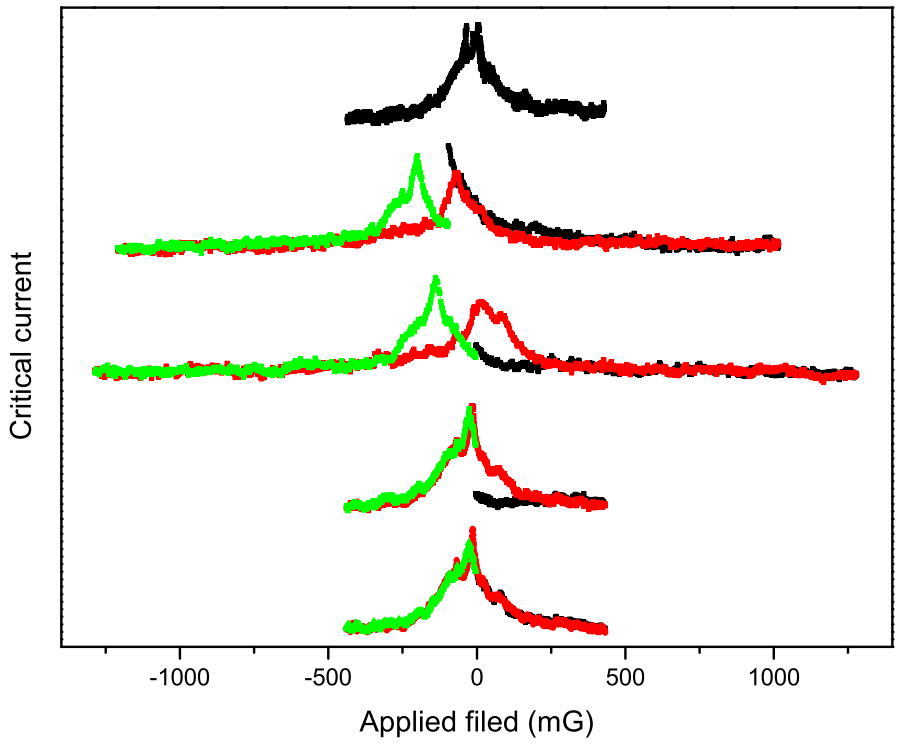

Figure 5.6 *Consecutive diffraction patterns from top to bottom in a Sr_2RuO_4 junction that show hysteresis and healing from it. As the maximum applied field is increased in the first three traces, the hysteresis loop opens up more. The maximum ramp field is then decreased to its original value for the last two traces and the patterns go back to retracing. The colors indicate the order in which the field sweep were made: black, red and then green.*

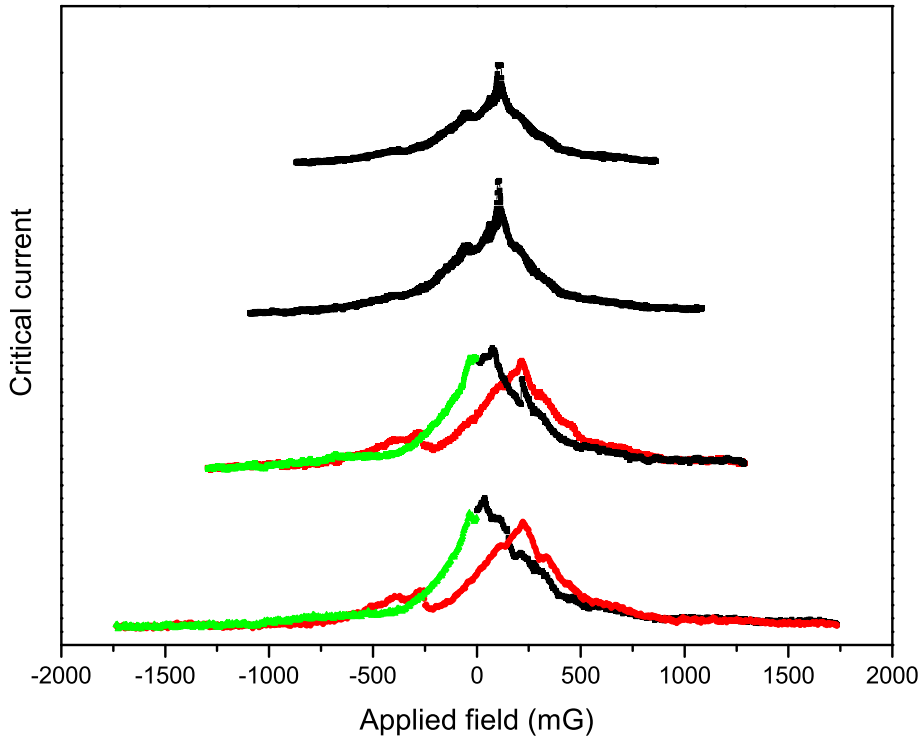

Figure 5.7 *Consecutive diffraction patterns showing discrete hysteresis in Sr_2RuO_4 junctions. Once the threshold field value is passed, the amount of hysteresis remains the same until the next threshold is passed.The colors indicate the order in which the field sweep were made: black, red and then green.*

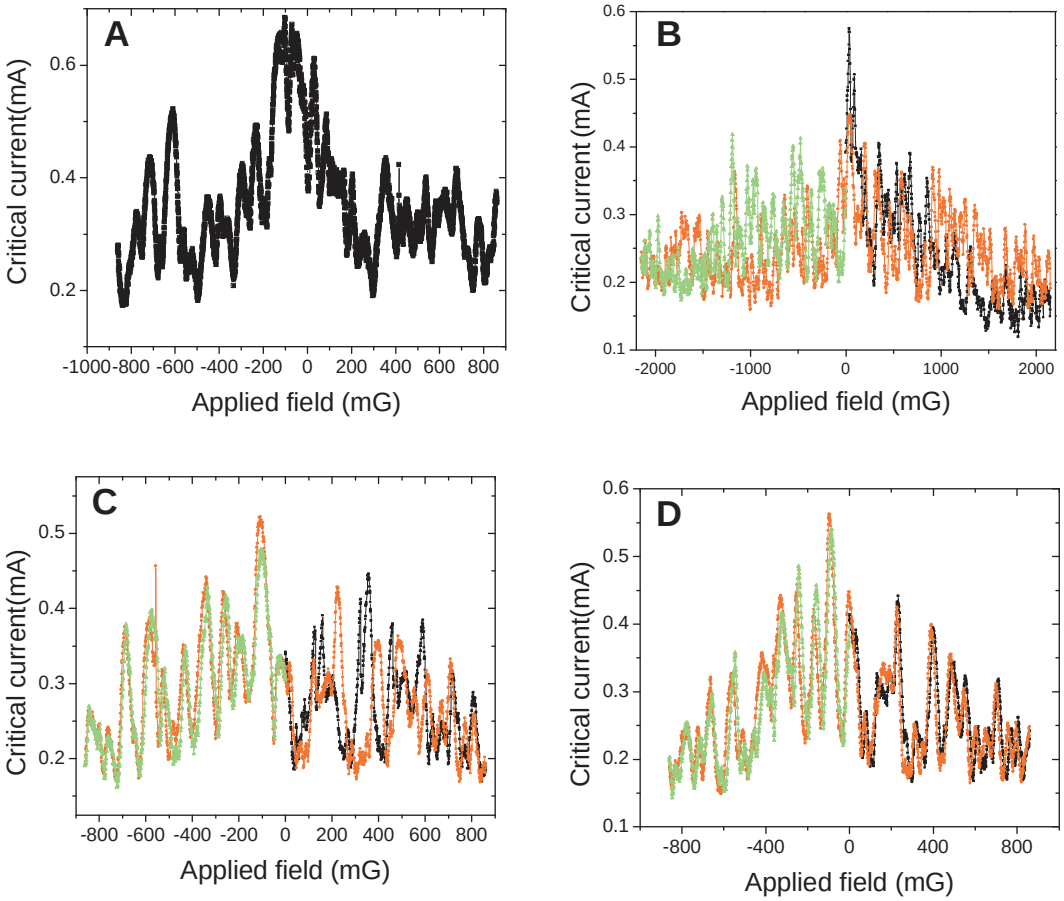

Figure 5.8 *Change in the diffraction pattern after a high field sweep. (A) Before field sweep; (B) Field sweep to 2G, above the hysteresis threshold; (C) First trace after high field is half retracing, half hysteretic and different from original pattern; (D) Pattern goes back to retracing but different from original.The colors indicate the order in which the field sweep were made: black, red and then green.*

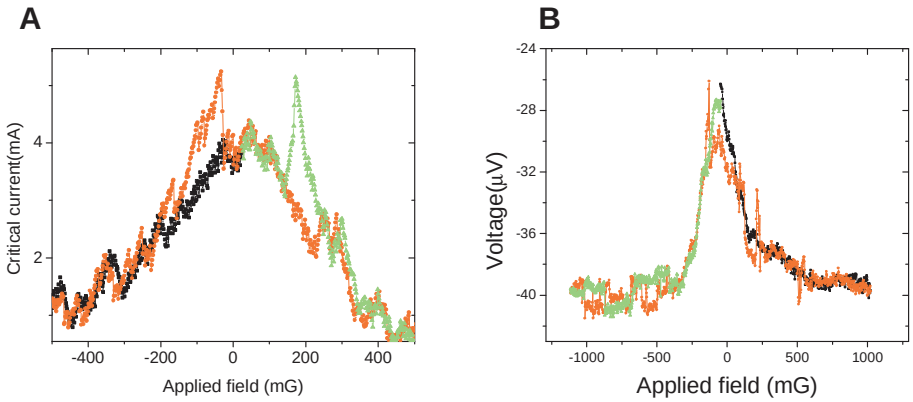

Figure 5.9 *Switches in the diffraction pattern as field is applied to the junction. (A) Isolated switching events, almost symmetric in field; (B) Telegraph noise. The colors indicate the order in which the data was taken: first black, the red and finally green.*

5.3.2 Switches in the diffraction pattern

In some junctions, switches between different critical current values occur in the diffraction patterns. In rare occasions, they are symmetric for positive and negative field. They seem to be switches between two states with different critical current, one stable at low field and the other stable at high field (see Fig.5.9 (A)). We sometimes observe multiple switches, telegraph noise between two metastable critical current states (see Fig.5.9 (B)). For different sweeps, the switches are usually reproducible within a narrow field range and that range is sample dependent. Both types of switches are affected by thermally-cycling the junctions to above the T_c of Sr_2RuO_4.

Switches also occur with time at a constant field, although we have only observed this after a field sweep. Sometimes we only observe a few jumps before the system relaxes into a stable state (see Fig.5.10(A)), but in other cases we see telegraph behavior as for a bi-stable system (see Fig.5.10 (B)). The timescale of the switches is typically on the order of seconds.

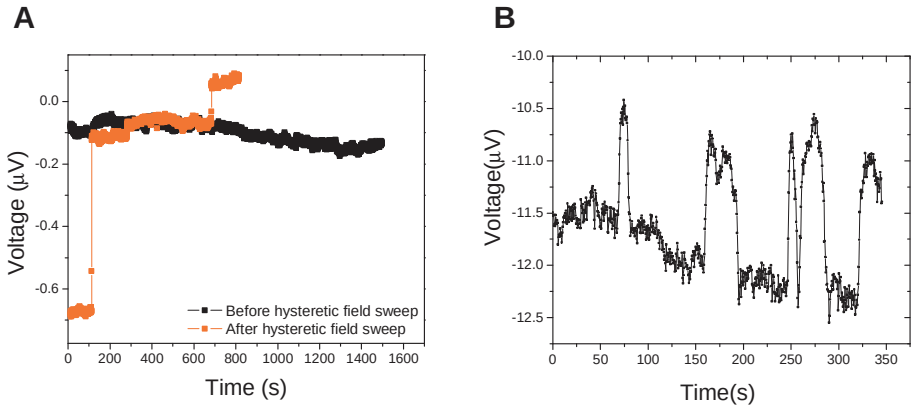

Figure 5.10 *Switches in diffraction pattern at constant applied field. (A)Relaxation to a stable state, (B) telegraph noise.*

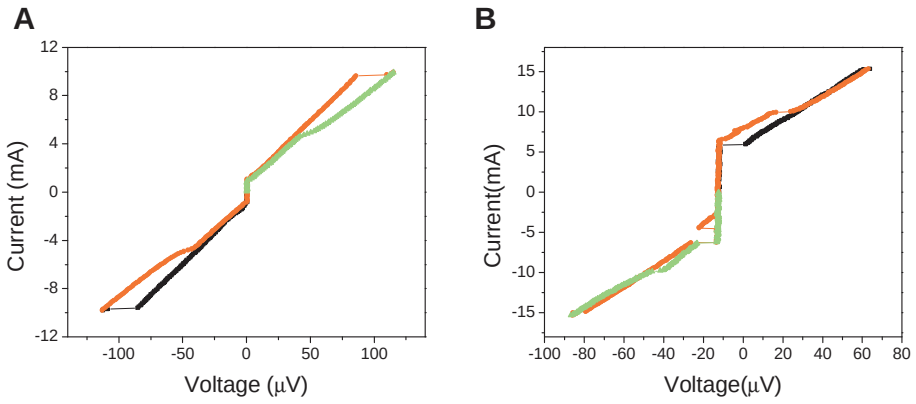

Figure 5.11 *Switching in the IV characteristics of the junctions. (A) Single switch at high current; (B) multiple two-level-type switching. The colors indicate the order in which the field sweep was made: black, red and then green.*

5.3.3 Switches in the IV

We also observed two types of switches in the IV characteristics of junctions. First, a second switch in the IV was observed every time a high current (I $\geq$ 6mA) was applied to a junction (see Fig.5.11 (A)). Its temperature dependence is very different from that of the critical current: it goes to a high value right below T_c and remains almost constant at lower temperatures. That indicates that the second switch doesn't come from the junction. The second type is a two-level telegraph type of switching as described for other physical quantities. It is more rare, observed only in two junctions, but when

present in a junction it is reproducible and survives thermal cycling. It can be triggered by a magnetic field. An example is given on Fig.5.11 (B).

There are a number of possible causes of these switches: heating, exceeding the critical current of one of the superconductors, vortex or domain wall motion could cause them. Heating would originate from the resistive components of the circuit and heat one or both superconductors to above their superconducting transition temperature. If the switches were caused by heating, the position of the second switch would depend on the speed of the current sweep. A slower sweep would cause power to dissipate longer and hence more heating while a faster sweep would cause less heating and the switch would occur at a higher current value. In the experiment, the position of the switch was independent of how fast the current was ramped. A more convincing argument against part of the sample becoming normal through either heating or exceeding the critical current is that some of the switches (e.g., see Fig.5.11 (B)) decrease the junction's resistance. Vortices or domain wall motion are possible causes of the switches. As mentioned earlier, it is hard to distinguish effects caused by these two.

5.3.4 Discussion

We interpret both the hysteresis and the switches in the data as evidence for domain dynamics: changes in the configuration of the order parameter domains that are reflected in the junction's critical current. Reversing the chirality of a single domain, reorienting the real part of a domain or, most likely, moving a domain wall, can all dramatically affect the critical current. This is demonstrated in Fig.5.12 (A), in which we compare the diffraction pattern for a junction with 10 parallel chiral domains to one for which a single domain wall is slightly displaced. Note that they are quantitatively similar

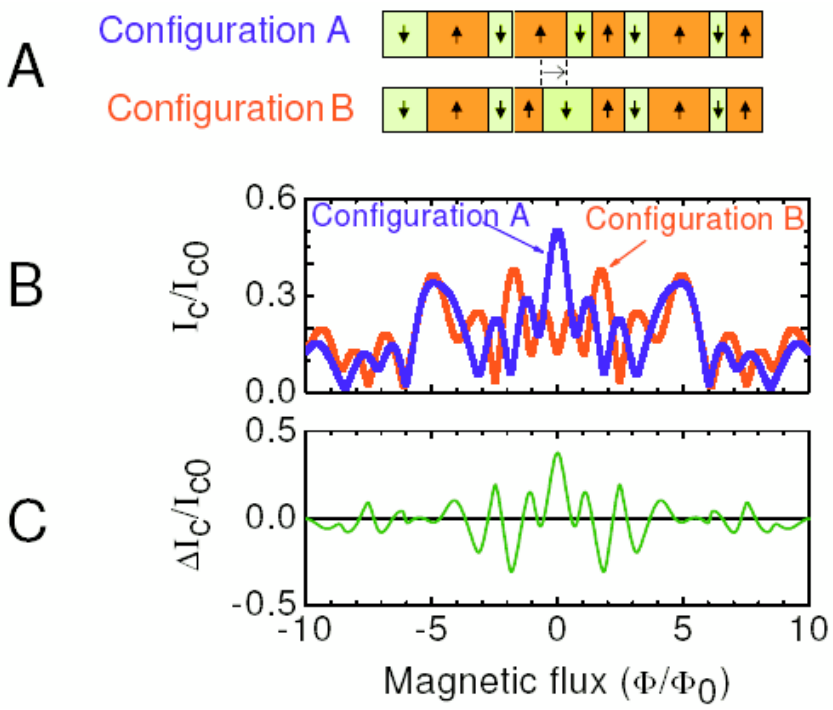

Figure 5.12 *(A) Schematic of chiral domain structures A and B which differ by the displacement of a single parallel domain wall. The up and down arrows indicate the chirality of each domain. (B) Calculated critical current diffraction patterns for domain configurations A and B. (C) Change in critical current for the domain wall shift as a function of applied magnetic flux through the junction.*

(Fig.5.12 (B)), but the critical current at any applied magnetic field value is significantly changed (Fig.5.12 (C)). Reversing the chirality of a single domain has a similar effect. Thus, abrupt switches in the critical current can arise if the domain orientations or domain wall locations change. These can be thermally-activated, giving rise to the telegraph switching noise at a fixed magnetic field.

An applied magnetic field can induce transitions between chiral domain configurations. Because magnetic fields couple to the chiral order parameter state, an applied magnetic field lifts the degeneracy between chiral domains, causing one of the chiralities to be favored over the other. Hence, the field will cause domain walls to move in order to enlarge the favored domains. In

practice, the domain walls may not move freely because of pinning at defects in the crystal structure, impurities, or other regions of weakened superconductivity. When a magnetic field is applied to the sample, the force on the domain walls only causes them to move if it exceeds the domain pinning potential. Once unpinned, the domain walls can either move smoothly or jump from pinning site to pinning site with increasing field, depending on the distribution of pinning sites in the course of motion. Because the domain structure can change as the field is swept, the magnetic field modulation curves might not correspond to a single domain configuration but instead can be a compilation of many. When the magnetic field is ramped up and then back down, the junction may end up in a distinctly different domain configuration, leading to hysteresis. The change in the patterns after a hysteretic sweep can be explained by considering the domain configuration as representing a local minimum of the free energy; there are other configurations with comparable or lower energy. When a large field is applied, the domain configuration is changed and, when the field is turned off, the system will settle in a low energy domain configuration that is different from the initial one.

We have also considered if vortex entry and motion could explain all of our data, as this phenomenon shares many of the same properties with domain dynamics: vortices can distort the diffraction pattern, induce field asymmetry, and move in and out of the junctions causing dynamics. One significant difference is that domains are intrinsic to the system and should always be expected to form, whereas vortices arise from external conditions during cooldown so that careful magnetic shielding together with slow cooling should considerably lower their probability of occurrence. To monitor this, each sample was thermally cycled at least 5 times to above the transition

temperature. The results showed consistency from one cycle to another, aside from small variations in critical current magnitude and period of modulation and, in some cases, the appearance and disappearance of hysteresis. Also, the dynamics were found to be highly reproducible, which in our experience is not the case for vortices. Another difference is their behavior in a bipolar field sweep. For accidentally trapped isolated vortices, field induced events are not symmetric for positive and negative field since the vortex has a specific polarity. In the case of domains, different polarities favor different chiralities and both field directions should induce dynamics at the same scale. Data like Fig.5.9 (A) is hard to explain with vortices since the switches occur at field values close in magnitude for both polarities. Thus, we are confident that vortices cannot account for our results but in general caution that this effect must always be carefully considered in interpreting Josephson interferometry data.

6 Cooling in a magnetic field

6.1 Simulations and experimental results

A good test for the presence of order parameter domains in Sr_2RuO_4 is cooling the junctions in a magnetic field parallel to the c-axis of the crystal. The two chiral order parameters couple to the field and their degeneracy is lifted. One is favored by a positive field while the other is favored by a negative field. Computer simulations of diffraction patterns when one type of domain is more probable than the other are given in Fig.6.1. Here, P_L and P_R are the probability of presence of left- and right-handed chiral domains in the material. As one of the chiralities become more probable, the magnitude of the critical current increases. We performed the experiment, using the magnitude of the critical current as a measure of domain alignment.

This is a challenging experiment because when a junction is cooled in a magnetic field, vortices are trapped in the sample and as mentioned before they distort the diffraction patterns. Hence a field cooled junction will show the combined effect of domain alignment and trapped magnetic field; depending on whether and where the vortices are trapped, the critical current enhancement might not be observable. However, when the enhancement is observed, it is evidence for domain alignment. We performed the experiment at various field values in the mG range but found that a noticeable effect was only achieved at much lower fields in the $10-100\mu G$ range. The enhancement was observed for four samples for both positive and negative fields, as shown

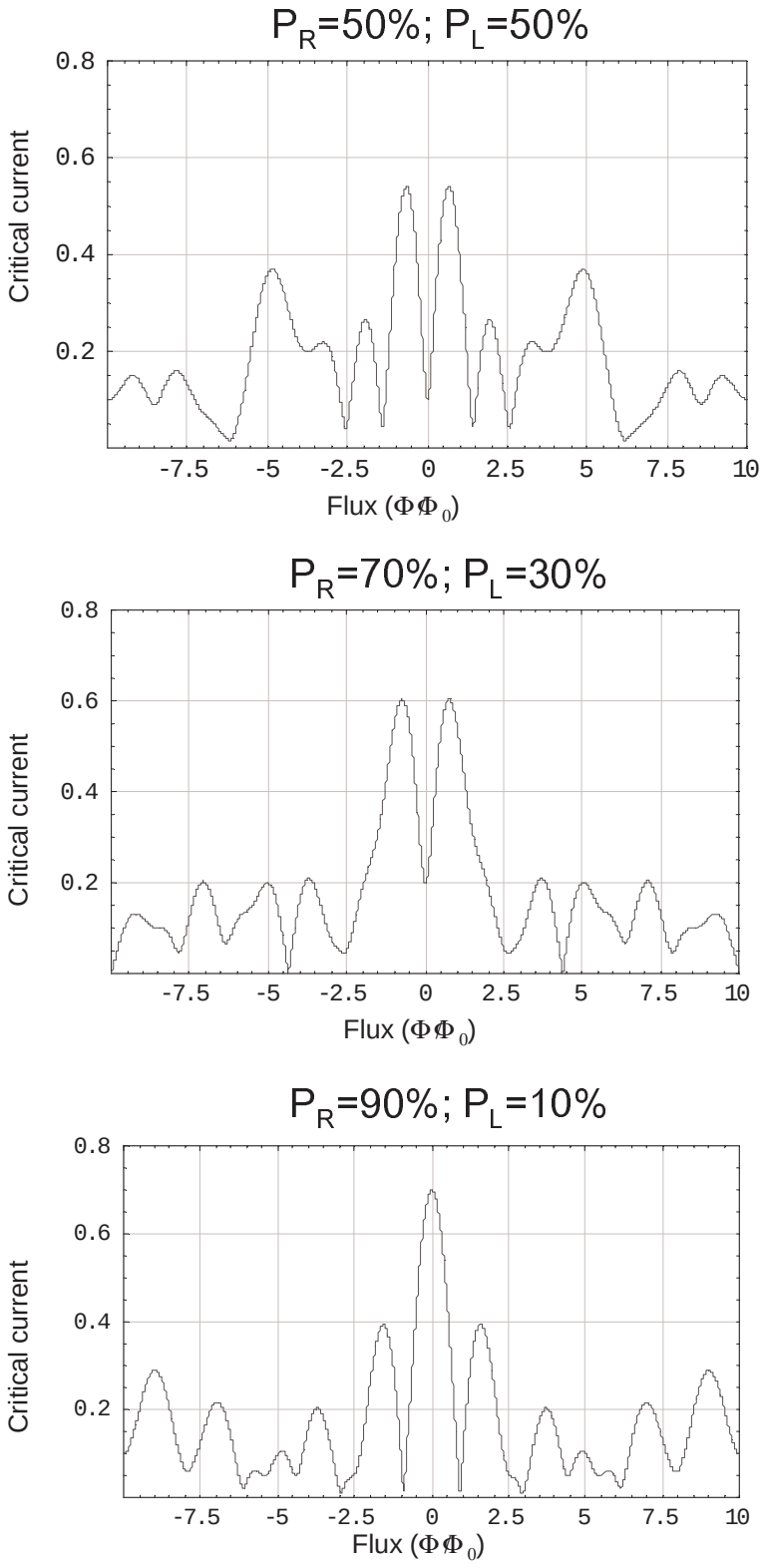

Figure 6.1 *Simulation of diffraction patterns of a junction where the probability of finding right handed chiral domains is of* 50%, 70% *and* 90% *as shown on the figure.*

in Fig.6.2. This is very strong evidence for the presence of order parameter domains.

6.2 Complicating factors

Although the data shows the critical current enhancement, in agreement with the simulations, some aspects of it are hard to understand.

First, we address a memory effect observed in the data. Once the critical current of the junction is enhanced, it retains a high value even when warmed above the transition temperature of all superconductors on the sample. The system seems to remember that it was previously cooled in a field. Moreover, the enhanced critical current onsets gradually, as if the system was being "trained" to remember that it was field cooled. The data showing evidence of these two phenomena is given in Fig.6.3. The memory effect is obviously unrelated to the superconductivity in the material and is probably the result of the very rich magnetic behavior in the ruthenate family. The system relaxes with time and temperature, but at temperatures as high as $77K$ and times as long as 24h, the memory is not erased: as can be seen in Fig.6.4 the critical current is lower than right after the field cooling but still much higher than in the original state. We have not determined the conditions under which the domain structure randomizes.

The second aspect that is hard to understand is that we find that there is a range in magnetic field at which large critical current enhancements are observed. Even though we were able to observe the effect in four samples, we had to comb through a large range of fields for each sample before we could find the field that would cause the maximum enhancement. This can be understood to some extent although not completely. The correct field has

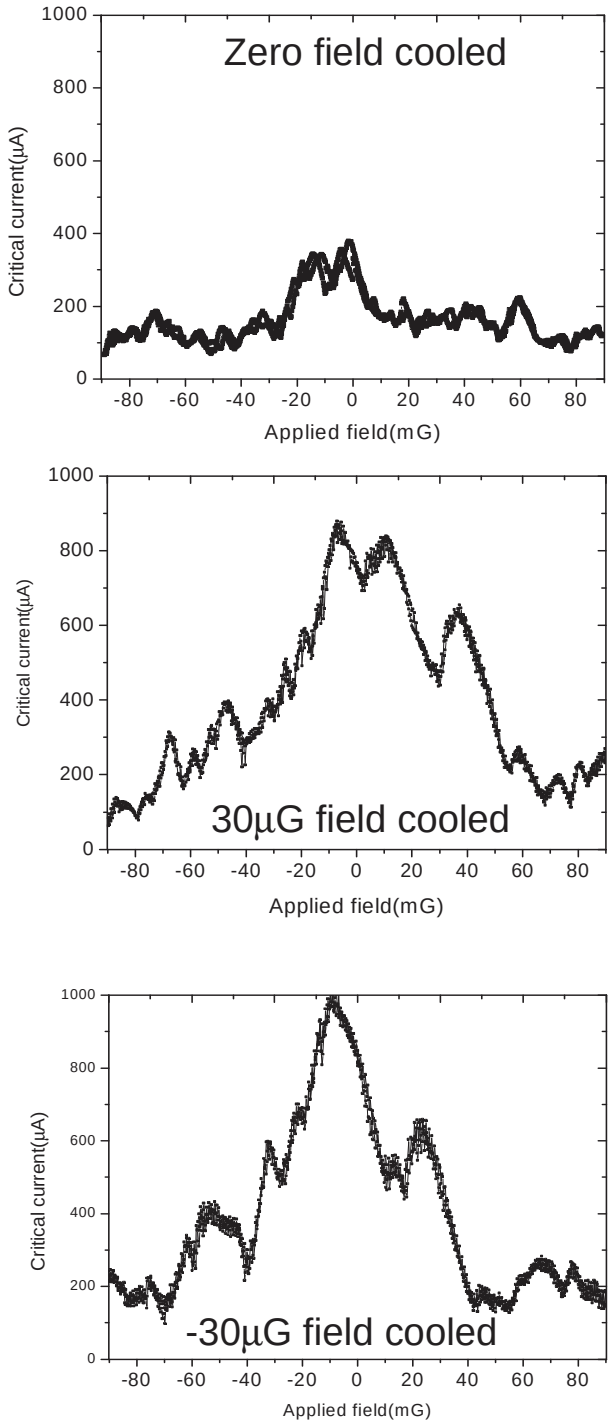

Figure 6.2 *Enhancement of the critical current by field cooling in a $Sr_2RuO_4/Cu/Pb$ junction. The zero field cooled junction has a critical current that is less than half of that of the same junction cooled in a field.*

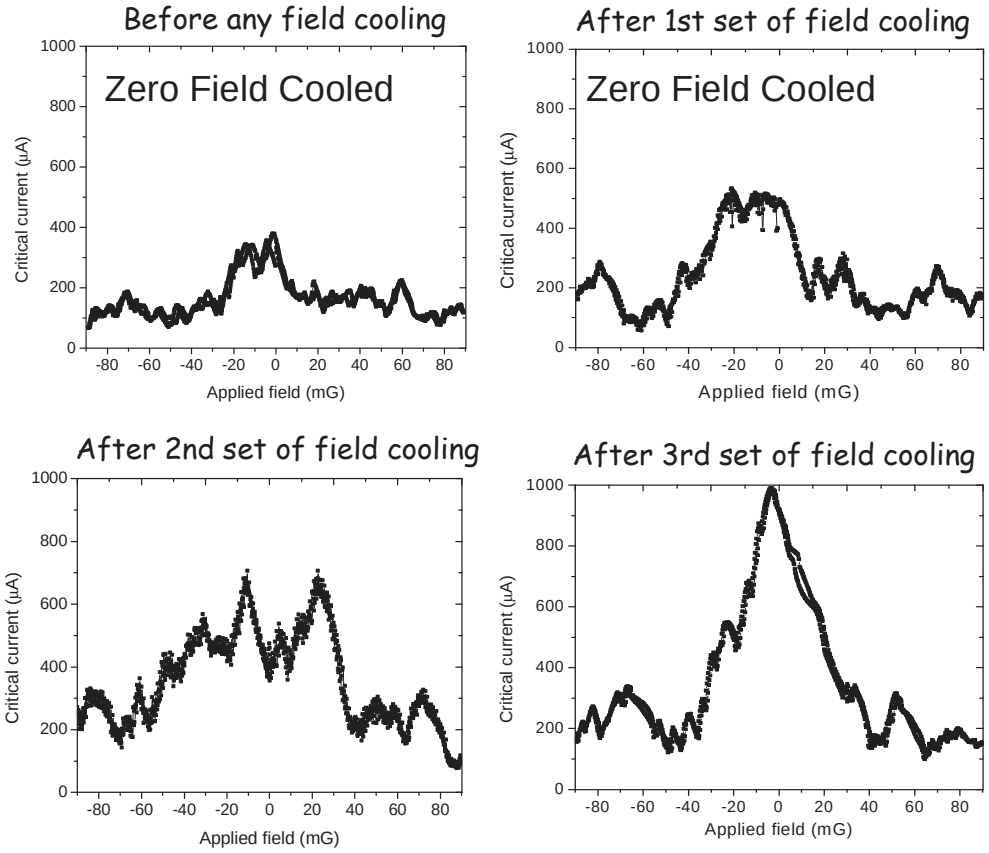

Figure 6.3 *Critical current enhancement in zero field cooled junctions. I_c is more and more enhanced as the number of iterations increases.*

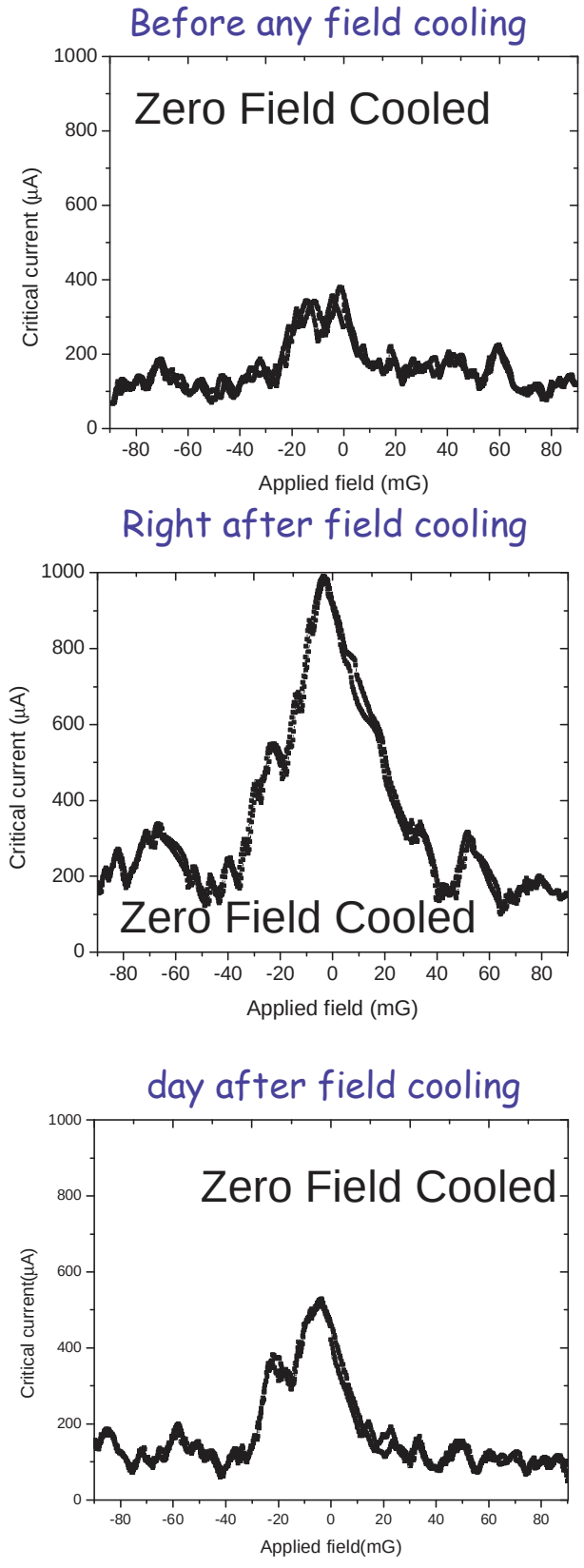

Figure 6.4 *Relaxation of the memory effect with time and temperature. The bottom trace was taken* 20*h later than the middle one, and the junction had warmed up to* 77K.

to be large enough to split the degeneracy between the two order parameters yet remain small to avoid vortices. Also, the exact domain configuration before and after field cooling dictates how much of the effect we observe and introduces a sample specific dimension to the problem. However, none of this explains why such small fields, in many cases comparable to residual background fields, can have such a significant effect.

The lack of independent measures of the domain alignment and the magnetic behavior causing the memory limited the scope of our investigation. The memory effect made it impossible to properly characterize the field cooling effect on domains. Properties such as the dependence of the critical current enhancement on the applied field couldn't be obtained since the enhancement depends not only on the applied field for a specific cooling but also on all previous field cooling iterations. On the other hand, because the only measure of the magnetic behavior was the magnitude of the critical current, a property only present in the superconducting state and that depends on more factors than just the magnetic behavior, it also became impossible to characterize the source of the memory effect.

7 Conclusions and future work

We report direct evidence for the presence of order parameter domains and domain wall motion in Sr_2RuO_4 through the anomalous behavior of diffraction patterns of Josephson junctions made on single faces of the crystal. This result is based on the study of critical current diffraction patterns from over 30 $Sr_2RuO_4/Cu/Pb$ junctions, each of which demonstrated some or all of the described unusual features, including complicated modulations characteristic of interference between regions with different phase and size, distinctly different behavior in different crystals and even in different junctions on the same crystal, asymmetry with respect to field direction, abrupt jumps in the critical current, and telegraph switching noise. We propose two families of domains to interpret the data: parallel chiral domains in which only the direction of the phase winding changes and perpendicular chiral domains in which the chirality and the orientation of the real part of the order parameter both change. The strikingly different diffraction patterns for junctions on orthogonal faces of the same single crystal confirm both the odd pairing symmetry and the broken time reversal symmetry of Sr_2RuO_4.

A key test is to determine if the chiral domains can be aligned by cooling in a magnetic field which favors a particular chiral state. We have done measurements indicating that cooling in even small fields ($\leq$ 1mG) can enhance the zero field critical current substantially (by up to a factor of two) and make the diffraction pattern more Fraunhöfer-like. We note that the field scale over which we can explore this effect is very restricted since larger fields

induce magnetic vortex entry and trapping in the vicinity of the junctions, creating local inhomogeneous fields that dramatically modify the diffraction patterns. Nonetheless, we do find evidence for coupling of a magnetic field to the domain structure, strong support for chiral symmetry.

The presence of order parameter domains in superconductors opens a new door into the field and more work will need to be done to completely understand the observed behavior. We propose here a few experiments that would further the understanding of that novel state and help assess the possibility of applications. The conclusions made here stem from the compilation of a large body of evidence. A "smoking gun" experiment using Josephson interferometry would require making a junction small enough to be within one domain, then slowly increase the junction size. In doing so, the diffraction pattern would go from Fraunhöfer and gradually turn into a multiple phase interference pattern. Measurements of the current-phase relation and Shapiro steps in the junction would answer the question of whether or not these junctions are pi-junctions, i.e., Josephson junctions whose lower energy state maintains a π phase shift across the junction. Another interesting experiment would be putting a magnetic barrier in the junction in an effort to understand the coupling between singlet and triplet superconducting states. Current switches based on triplet superconductor/ferromagnet/singlet superconductor have been proposed.

Experiments to understand the "memory effect" in the field cooling experiments would also be desirable. Finding the transition temperature of the magnetic phase associated with the relaxation of the memory fields would allow a better characterization of the domain alignment by field cooling.

Appendices

A List of samples measured in the experiment

Sample name	Central peak	Hysteresis	Healing	Switches with field	Switches in time	Junctions on 2 sides	Field cooling
F021704						YES	
JCT1	YES	YES	YES	NO	NO		NO
JCT3	NO	YES	YES	NO	NO		NO
F042005						YES	
JCT1	YES	YES	YES	YES	NO		NO
JCT2	NO	NO	NO	YES	NO		NO
F042804	NO	NO	NO	NO	NO	NO	NO
F071405						NO	
JCT1	NO	YES	NO	YES	NO		NO
JCT2	NO	NO	NO	NO	NO		NO
F082005						NO	
JCT1	NO	YES	YES	YES	YES		NO
JCT3	YES	YES	YES	YES	YES		NO
F080504	YES	YES	YES	YES	YES	NO	NO
F090904	NO	NO	NO	NO	NO	NO	NO
F092804	NO	NO	NO	NO	NO	NO	NO
F111604						NO	
JCT1	NO	YES	NO	NO	NO		NO
JCT2	NO	YES	NO	NO	NO		NO
JCT3	NO	YES	NO	NO	NO		NO

Sample name	Central peak	Hysteresis	Healing	Switches with field	Switches in time	Junctions on 2 sides	Field cooling
F120104						NO	
JCT1	NO	YES	NO	NO	YES		NO
JCT2	NO	NO	NO	YES	YES		NO
JCT3	NO	YES	NO	YES	NO		NO
JS012405	NO	YES	YES	NO	NO	NO	NO
JS070705						YES	
JCT1	NO	NO	NO	NO	NO	SIDE 1	NO
JCT2	NO	NO	NO	NO	NO	SIDE 1	YES
JCT3	NO	NO	NO	NO	NO	SIDE 1	NO
JCT4	NO	YES	NO	NO	NO	SIDE 1	YES
JCT5	NO	NO	NO	NO	NO	SIDE 2	NO
JCT6	NO	NO	NO	NO	NO	SIDE 2	NO
JCT7	NO	NO	YES	NO	NO	SIDE 2	NO
F022006						NO	
JCT1	NO	YES	NO	NO	YES		YES
JCT2	NO	YES	YES	YES	YES		YES
F042406	NO	YES	NO	YES	NO	NO	NO
F051506						YES	
JCT2	NO	YES	NO	YES	NO		YES
JCT3	NO	YES	NO	YES	NO		YES

References

[1] V. L. Ginzburg and L. D. Landau *Zh. Eksperim. i. Teor. Fiz.*, vol. 20, p. 1064, 1950.

[2] J. Bardeen, L. N. Cooper, and J. R. Schrieffer *Phys. Rev.*, vol. 108, p. 1175, 1957.

[3] A. P. Mackenzie and Y. Maeno *Rev. Mod. Phys.*, vol. 75, p. 657, 2003.

[4] R. Matzdorf, Z. Fang, Ismail, J. Zhang, T. Kimura, Y. Tokura, K. Terakura, and E. W. Plummer *Science*, vol. 289, p. 746, 2000.

[5] T. Oguchi *Phys. Rev. B*, vol. 51, p. 1385, 1995.

[6] A. P. Mackenzie, N. E. Hussey, A. J. Diver, S. R. Julian, Y. Maeno, S. Nishizaki, and T. Fujita *Phys. Rev. B*, vol. 54, p. 7425, 1996.

[7] C. Bergemann, J. S. Brooks, L. Balicas, A. P. Mackenzie, S. R. Julian, Z. Q. Mao, and Y. Maeno *Physica B*, vol. 294, p. 371, 2001.

[8] T. Imai, A. W. Hunt, K. R. Thurber, and F. C. Chou *Phys. Rev. Lett.*, vol. 81, p. 3006, 1998.

[9] Y. Sidis, M. Braden, P. Bourges, B. Hennion, W. Reichardt, Y. Maeno, and Y. Mori *Phys. Rev. Lett.*, vol. 83, p. 3320, 1999.

[10] S. Nishizaki, Y. Maeno, and T. Fujita *J. Phys. Soc. Jpn.*, vol. 65, p. 1876, 1996.

[11] K. Ishida, Y. Kitaoka, K. Asayama, S. Ikeda, S. Nishizaki, Y. Maeno, K. Yoshida, and T. Fujita *Phys. Rev. B.*, vol. 56, p. R505, 1997.

[12] P. W. Anderson *Phys. Rev. Lett.*, vol. 3, p. 325, 1959.

[13] R. Balian and N. R. Werthamer *Phys. Rev.*, vol. 131, p. 1553, 1963.

[14] A. I. Larkin *JETP Lett.*, vol. 2, p. 130, 1965.

[15] A. P. Mackenzie, R. K. W. Haselwimmer, A. W. Tyler, G. G. Lonzarich, Y. Mori, S. NIshizaki, and Y. Maeno *Phys. Rev. Lett.*, vol. 80, p. 161, 1998.

[16] A. P. Mackenzie, R. K. W. Haselwimmer, A. W. Tyler, G. G. Lonzarich, Y. Mori, S. NIshizaki, and Y. Maeno *Phys. Rev, Lett.*, vol. 80, p. 3890, 1998.

[17] Z. Q. Mao, Y. Mori, and Y. Maeno *Phys. Rev. B.*, vol. 60, p. 610, 1999.

[18] Z. Q. Mao, Y. Maeno, Y. Mori, S. Sakita, S. Nimori, and M. Udagawa *Phys. Rev. B*, vol. 63, p. 144514, 2001.

[19] T. Akima, S. Nishizaki, and Y. Maeno *J. Phys. Soc, Jpn.*, vol. 68, p. 694, 1999.

[20] S. Nishizaki, Y. Maeno, and Z. Q. Mao *J. Low Temp. Phys.*, vol. 117, p. 1581, 1999.

[21] M. Sigrist and K. Ueda *Rev. Mod. Phys.*, vol. 63, p. 231, 1991.

[22] J. F. Annett *Physica C*, vol. 317-318, p. 1, 1999.

[23] M. Tinkham, *Introduction to Superconductivity: 2nd Ed.* McGraw Hill, 1996.

[24] K. Ishida, H. Mukuda, Y. Kitaoka, K. Asayama, Z. Q. Mao, Y. Mori, and Y. Maeno *Nature*, vol. 396, p. 658, 1998.

[25] K. Ishida, H. Mukuda, Y. Kitaoka, Z. Q. Mao, H. Fukazawa, and Y. Maeno *Phys. Rev. B*, vol. 63, p. 060507, 2001.

[26] G. M. Luke, Y. Fudamoto, K. M. Kojima, M. I. L. J. Merrin, B. Nachumi, Y. J. Uemura, Y. Maeno, Z. Q. Mao, Y. Mori, H. Nakamura, and M. Sigrist *Nature*, vol. 394, p. 558, 1998.

[27] J. A. Duffy, S. M. Hayden, Y. Maeno, Z. Mao, J. Kulda, and G. J. McIntyre *Phys. Rev. Lett*, vol. 85, p. 5412, 2000.

[28] K. D. Nelson, Z. Q. Mao, Y. Maeno, and Y. Liu *Science*, vol. 306, p. 1151, 2004.

[29] P. G. Kealey, T. M. Riseman, E. M. Forgan, A. P. Mackenzie, L. M. Galvin, S. L. Lee, D. McK. Paul, R. Cubitt, D. F. Agterberg, R. Heeb, Z. Q. Mao, and Y. Maeno *Phys. Rev. Lett.*, vol. 84, p. 6094, 2000.

[30] J. Xia, Y. Maeno, P. T. Beyersdorf, M. M. Fejer, and A. Kapitulnik *cond-mat*, vol. 0607539, 2006.

[31] T. M. Rice and M. Sigrist *J. Phys. Cond. Mat.*, vol. 7, p. L643, 1995.

[32] K. Deguchi, Z. Mao, and Y. Maeno *J. Phys. Soc. Jpn*, vol. 573, p. 1313, 2004.

[33] D. F. Agterberg, T. M. Rice, and M. Sigrist *Phys. Lett.*, vol. 78, p. 3374, 1997.

[34] G. E. Volovik and L. P. Gor'kov *Sov. Phys. JETP*, vol. 61, p. 843, 1985.

[35] G. E. Volovik and L. P. Gor'kov *JETP Lett.*, vol. 39, p. 674, 1984.

[36] M. Sigrist, T. M. Rice, and K. Ueda *Phys. Rev. Lett.*, vol. 63, p. 1727, 1989.

[37] M. Matsumoto and M. Sigrist *J. Phys. Soc. Jpn.*, vol. 68, p. 994, 1999.

[38] A. Amann, A. C. Mota, M. B. Maple, and H. v.Löhneysen *Phys. Rev. B*, vol. 57, p. 3640, 1998.

[39] E. Dumont, A. C. Mota, and J. L. Smith *J. Low Temp. Phys.*, vol. 117, p. 1477, 1999.

[40] A. C. Mota, E. Dumont, A. Amann, and Y. Maeno *Physica B*, vol. 259-261, p. 934, 1999.

[41] M. Sigrist and D. F. Agterberg *Prog. Theor. Phys.*, vol. 102, p. N.5, 1999.

[42] V. O. Dolocan, C. Veauvy, F. Servant, P. Lejay, K. Hasselbach, Y. Liu, and D. Mailly *Phys. Rev. Lett.*, vol. 95, p. 097004, 2006.

[43] J. R. Waldram, *Superconductivity of Metals and Cuprates*. Institute of Physics, 1996.

[44] A. Barone and G. Paternò, *Physics and Applications of the Josephson Effect*. John Wiley and sons, 1982.

[45] D. J. V. Harlingen *Rev. Mod. Phys.*, vol. 67, p. 515, 1995.

[46] D. A. Wollman, D. J. V. Harlingen, W. C. Lee, D. M. Ginsberg, and A. J. Leggett *Phys. Rev. Lett.*, vol. 71, p. 2134, 1993.

[47] D. A. Wollman, D. J. V. Harlingen, W. C. Lee, D. M. Ginsberg, and A. J. Leggett *Phys. Rev. Lett.*, vol. 73, p. 1872, 1994.

[48] D. A. Wollman, D. J. V. Harlingen, J. Giapintzakis, D. M. Ginsberg, and A. J. Leggett *Phys. Rev. Lett.*, vol. 74, p. 797, 1995.

[49] H. Hilgenkamp and J. Mannhart *Rev. Mod. Phys.*, vol. 74, p. 485, 2002.

[50] W. K. Neils, *Josephson Interferometry Measurements in High-Tc Grain Boundary Junctions*. PhD thesis, University of Illinois at Urbana-Champaign, 2002.

[51] J. A. Pals, W. van Haeringen, and M. H. van Maaren *Phys. Rev. B*, vol. 15, p. 2592, 1977.

[52] E. W. Fenton *Solid State Comm.*, vol. 54, p. 709, 1985.

[53] V. B. Geshkeinbein and A. I. Larkin *JETP Lett.*, vol. 43, p. 395, 1986.

[54] Y. Asano, Y. Tanaka, M. Sigrist, and S. Kashiwaya *Phys. Rev. B*, vol. 67, p. 184505, 2003.

[55] V. B. Geshkenbein, A. I. Larkin, and A. Barone *Phs. Rev. B*, vol. 36, p. 235, 1987.

[56] Y. Asano, Y. Tanaka, M. Sigrist, and S. Kashiwaya *Phs. Rev. B*, vol. 71, p. 214501, 2005.

[57] Z. Q. Mao, Y. Maeno, and H. Fukazawa *Mat. Res. Bul.*, vol. 35, p. 1813, 2000.

[58] D. Wollman, *Experimental determination of the symmetry of the superconducting pairing state in YBCO.* PhD thesis, University of Illinois at Urbana-Champaign, 1996.

[59] F. Kidwingira, J. D. Strand, D. J. V. Harlingen, and Y. Maeno *Science*, vol. 314, p. 1267, 2006.

Author's biography

Françoise Kidwingira was born on July 1st 1975 in Bujumbura, Burundi. Upon high school graduation in 1993, she attended the "Université du Burundi". She earned a "Licence en science physique", the equivalent of a Bachelor of science degree in physics, in July of 1999. Her senior research was in geophysics, on seismic ray tracing using the finite difference method. In the Fall of 1999, she enrolled in a master's program at Clark Atlanta University where she worked in an atomic physics group on the use of Stokes Lines to calculate Regge pole trajectories, which are used in the determination of small angle scattering cross sections. After a Summer internship in experimental condensed matter physics at the Georgia Institute of Technology, she decided to pursue the field and started her PhD at the University of Illinois in the Fall of 2001. She joined the research group of Dale Van Harlingen in January of 2002.